Texas A&M University
Mechanical Engineering Department
Turbomachinery Laboratory

MEASUREMENTS OF ROTORDYNAMIC PERFORMANCE IN A HOT ROTOR-GAS FOIL BEARING SYSTEM

Research Progress Report to the Turbomachinery Research Consortium

TRC-B&C-2-09

by

Luis San Andrés
Mast-Childs Professor
Principal Investigator

Keun Ryu
Research Assistant
Tae Ho Kim
Postdoctoral Research Associate

May 2009

MEASUREMENTS OF ROTORDYNAMIC PERFORMANCE IN A HOT ROTOR-GAS FOIL BEARING SYSTEM

Executive Summary

The TRC project co-sponsors a NASA GRC funded program on the development of computational models, experimentally benchmarked, for prediction of gas foil bearing performance at high temperature operation. Implementation of gas foil bearings (GFBs) into gas turbines requires careful thermal management and demands reliable performance measurements and predictions.

In 2009[1], measurements of bearing and rotor temperatures and shaft motions are obtained in a hot rotor supported on a pair of 2nd generation GFBs (uncoated top foils). A high speed AC motor (9.5 kW at 65 krpm) replaces the inexpensive router motor (1.5 kW at 25 krpm) used earlier. An inexpensive electric cartridge (max. 360°C), loosely installed inside the hollow rotor, is a heat source warming (unevenly) the rotor and its bearings. A shop air stream (max. 300 L/min & 23°C) forced axially into the bearings can be regulated to determine its effectiveness in cooling the rotor and bearings. A cover with layers of ceramic paper insulates the test rig from ambient conditions.

In rotor speed coast downs from 25 krpm and with a cold rotor, the amplitudes of rotor synchronous motion are proportional to the added imbalance masses. For operation with a hot shaft, the amplitude of rotor motion drops while crossing a (rigid body mode) critical speed. Large elapsed times (50~70 s) for rotor speed coast downs demonstrate airborne operation with little viscous drag, as is typical with gas bearings support systems.

In extended time tests, at 20 minute intervals, the rotor speed is set at 10 krpm, then at 20 krpm, and lastly at 29.3 krpm. The recorded bearing cartridge and rotor surface temperatures steadily increase with operating time. For operation without or with 50 L/min axial cooling, the temperatures of the bearing cartridges are almost identical. Note that the free end rotor surface shows the largest temperature raise as operation time and rotor speed increase. There is a significant axial thermal gradient (up to 50°C) from the rotor free end towards its drive end. The measurements show that the rotor has a temperature path paralleling that of the heater. The temperatures on the bearing cartridges, on the other hand, increase steadily with time.

---

[1] TRC funded the project in late January 2009. The experimental results hereby presented were obtained over a length of time larger than 4 months and at a cost higher than that funded by TRC.

In further tests, at a rotor speed of 29.3 krpm, a cooling gas stream, with increasing strength, controls the temperatures in the bearings and rotor. First, the peak temperature of the heater surface drops from 360ºC (without cooling) to 165ºC for a 150 L/min flow rates into each bearing. Since the heater power is limited, the rotor surface temperature quickly drops as the cooling flow advects heat from the whole test rig. The effect of a cooling flow, if turbulent in character, is most distinctive at the highest heater temperature (360°C). For operation at ambient or a lower heater temperature condition, however, the cooling flow stream demonstrates a very limited effectiveness.

In a gas turbine, gas bleed-off from the compressor is readily available to cool an oil-free hot rotor-GFB system. However, a too large cooling stream will reduce the engine efficiency. Therefore, later developments must focus on the determination of the minimum cooling stream needed for adequate thermal management.

To date the foil bearings remain operational, in spite of the severe rotor vibrations and large thermal gradients introduced into the test system. Future experiments will replace the bearings with *MiTi* Kololon® coated foil bearings able to support (higher) temperatures akin to those found in gas turbine engines (see Appendix A).

Appendix B details the test rig components and shows its cost at $ 43,243.1, with only $ 1,525 spent from TRC resources. NASA GRC funds and the PI incentive funds paid for the test rig which benefits the TRC members. In addition, KIST (Korean Institute of Science and Technology) donated several foil bearings and a test rotor for further tests at high temperature, see Appendix C. The donation, amounting to a value of ~$10,000, also benefits TRC.

Note to reader: PI edited fully the report (English grammar and semantics and technical content) prior to its release to TRC members.
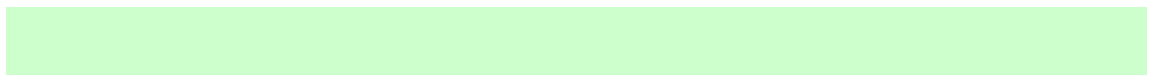
TABLE OF CONTENTS

LIST OF TABLES

LIST OF FIGURES

NOMENCLATURE

D_I	Bearing cartridge inner diameter [m]
D_O	Bearing cartridge outer diameter [m]
D_T	Top foil inner diameter [m]
h_B	Bump height [m]
L	Bearing axial length [m]
M_{DE} and M_{FE}	Fractions of the test rotor weight acting on each bearing [g]
m_i	Calibrated imbalance mass [g]
l_B	Bump length [m]
N_B	Number of Bumps [-]
r	Radial location of imbalance mass [m]
r_B	Bump arc radius [m]
s_0	Bump pitch [degree]
t_B	Bump foil thickness [m]
t_{BC}	Bearing cartridge wall thickness [m]
t_T	Top foil thickness [m]
$T_6 \sim T_9$	Drive end GFB cartridge outboard temperature [ºC]
T_{10}	Drive end bearing support housing surface temperature [ºC]
T_{11}	Free end rotor surface temperature [ºC]
T_{12}	Drive end rotor surface temperature [ºC]
T_{13}	Connecting rod temperature [ºC]
T_{14}	Drive motor inboard temperature [ºC]
T_{15}	Drive motor outboard temperature [ºC]
T_{16}	Drive motor support housing temperature [ºC]
T_{amb}	Test rig ambient temperature [ºC]
T_h	Cartridge heater temperature [ºC]
T_{hs}	Cartridge heater set temperature [ºC]
u	Mass imbalance displacement [m]
α	Bump arc angle [degree]

Acronyms

DH	Drive end, horizontal direction
DV	Drive end, vertical direction
FH	Free end, horizontal direction
FV	Free end, vertical direction
GFB	Gas foil bearing
MTM	Microturbomachinery

Introduction

Gas foil bearings (GFBs) enable micro-turbomachinery (MTM) operating at extreme conditions in rotational speed and temperature. These are compact units with reduced maintenance costs and operating with better mechanical efficiency and improved reliability [1]. Gas foil bearings offer distinct advantages over rolling elements bearings including no *DN* value limit, reliable high temperature operation, and large tolerance to debris and rotor motions (rubbing and misalignment) [2]. Current applications, commercialized or under development, include aircraft gas turbine engines, auxiliary power units, microturbines, pumps, compressors, cryogenic turboexpanders, and turbochargers, for example [3].

However, GFBs have demerits of excessive power losses and wear of protective coatings during frequent rotor startup and shutdown events. In addition, expensive developmental costs and, until recently, inadequate predictive tools have restricted the widespread deployment of GFBs into gas turbines, for example. Particularly, at high temperature conditions, reliable operation of GFB supported rotor systems relies on adequate engineered thermal management. The heat conducted from a hot turbine, for example, degrades the material properties and changes the bearing operating clearance[2] [4,5]. A cooling gas flow aids to carry away heat and prevent GFBs from encountering thermal seizure, thus maintaining an adequate load capacity and thermal stability [6]. High temperature endurance with wear resistance using solid lubricant coatings on the shaft and/or the top foil surface further aids to prevent bearing failure [7].

Since 2003, the gas foil bearing research program at TAMU has advanced experimentally validated computational tools predicting the static and dynamic forced performance of GFBs in high-speed turbomachinery. References [8-12] detail the research progress to date. In 2008, Kim and San Andrés [13] present rotordynamic measurements in a GFB test rig revamped for hot operation (max. heater temperature of 132ºC). An electric cartridge heater, rated at 250 W with 120 V, loosely installed inside the hollow rotor acts as a heat source. The shaft temperature increases with the heater temperature. Without heating, rotor speed-up tests show an abrupt drop in rotor amplitude of motion just above its critical speed, thus demonstrating a nonlinear system forced response attributed to a strong hardening effect of the GFB elastic support structure. As the heater temperature increases, due to the increase in the gas viscosity, the rotor motion peak amplitude decreases dramatically without amplitude jump for operation

---

[2] An excessive decrease in the operating clearance of the bearings increases the bearing power loss and decreases the bearing load capacity.

above the critical speed. Rotor speed coastdown tests from 26 krpm show that the system critical speed increases and the peak motion amplitude decreases significantly with shaft temperature. In spite of delivering large rates of cooling streams, up to ~56 L/min, the overall bearing temperature decreases just a few degrees (~5% less temperature that when operated without a cooling flow stream). References [13-16] review past work, experimental and analytical, on the performance of GFBs operating at high temperature.

The present work presents further rotordynamic tests for hot rotor operation spinning up to 30 krpm. The cartridge heater operates at a larger temperature, up to 360 ºC. A mass flow meter (max. 500 L/min) measures the forced cooling air stream into the test bearings. Steady state tests at a fixed rotor speed quantify the effect of the cooling flow strength on the bearing and rotor temperatures. Rotor speed coastdown tests evidence the effect of shaft temperature on the rotordynamic performance of the GFB supported rotor.

Experimental Facility

The GFB rotordynamic test rig detailed in Refs. [10, 17] is revamped for operation at high rotor speeds (max. 50 krpm) and with shaft temperatures to a max. of 400ºC. Figure 1 depicts the current configuration of the GFB test rig and its instrumentation. A pair of GFBs, housed in a massive steel base, supports a hollow rotor. The 210 mm long AISI 4140 rotor, 1.064 kg in mass and 4.8 mm thick, has a nominal outer diameter of 38.07 mm at the bearing locations (at room temperature). A thin dense Chrome coating[3] (3 µm thick), withstanding up to 500ºC, covers the rotor at the bearing locations.

A slender rod at one end of the rotor and a flexible coupling connect the rotor to a drive motor. The drive electric motor has two electromagnetic poles to produce 9.5 kW at its maximum operating speed of 65 krpm using a supply voltage of 400~460 VAC (3 phase, 50-60 Hz). According to the electric motor performance map, the motor has a torque of ~85 N-cm at a low speed of 6 krpm. The flexible coupling (35 mm in length, 25 mm in outer diameter, and 5.08 mm inner diameter) consists of a steel bellow and aluminum clamping hubs. The coupling rated (maximum service) torque and torsional stiffness are 2.0 N-m and 1200 N-m/rad, respectively. Note that the maximum operating temperature of the inexpensive coupling is 120°C.

An electric cartridge heater, fitting loosely inside the hollow rotor, acts as a steady source of thermal energy to heat the test rotor-bearing system. The cartridge heater has a nominal

---

[3] Multichrome/Microplate Certified Processing Lab, Inc deposited the coating at no cost.

diameter of 15.875 mm and overall length of 254 mm, and is rated at 1600 W when supplied with 240 VAC. Note that the heater does not warm evenly the rotor and test bearings, thus giving a significant axial temperature gradient along the rotor. See Appendix A for details.

An aluminum casing (7 mm thick) covers the whole test system and acts as a heat shield and safety enclosure to the test rig. Ceramic fiber paper (3.2 mm thick) insulates the inside walls of the casing. Fire-resistance mortar attaches the fiber paper to the casing walls. A gas flow meter, max. 500 L/min, records airflow streams into both foil bearings.

Figure 2 shows photographs of one of the test GFBs, 2nd generation, obtained from Foster-Miller Technologies. Table 1 lists the dimensions of the test bearings, each with uncoated top foil for high temperature operation. The test FB consists of a single arcuate top foil and five arcuate bump strip layers around the bearing circumference. Note that there are five other bump strip layers along the bearing axial length. Each bump strip, with five bumps, is spot welded at one end, and free at the other and. A bump strip spans 72° around the inner circumference of the bearing cartridge. The top foil is a conformed thin metal sheet welded to the bearing sleeve at one end, and free at the other end. The total number of bumps equals 125, i.e. 25 in the circumference of the bearing times 5 along its axial plane. The bearing cartridge is made of AISI 304 stainless steel, and the bump foils and top foils are made of Cr-Mb steel.

(a) Major components and instrumentation
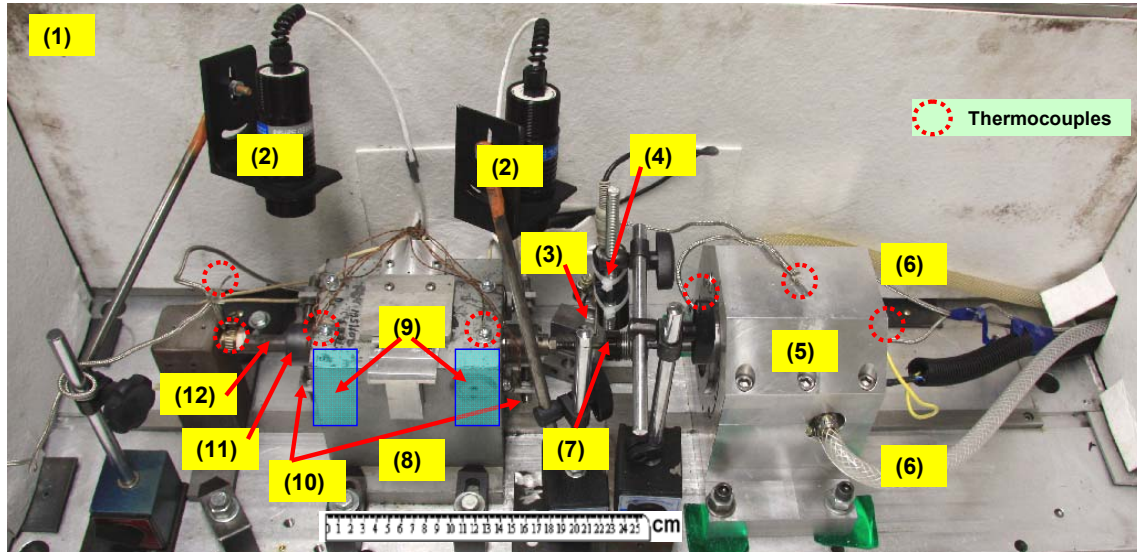
(1) Insulated safety cover
(2) Infrared thermometer
(3) Flexible coupling cooling air supply
(4) Infrared Tachometer
(5) Drive motor
(6) Motor cooling water supply

(7) Flexible coupling
(8) GFB support housing
(9) Test GFBs
(10) Displacement sensors
(11) Test hollow shaft
(12) Cartridge heater
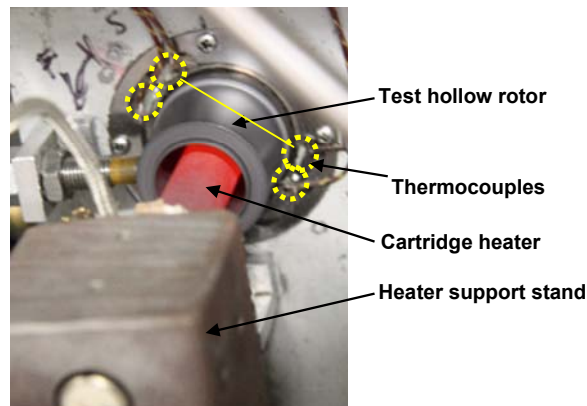
(b) Hot cartridge heater (T_{hs}=360ºC) and rotor spinning at 30 krpm

Fig. 1 Photograph of high temperature GFB rotordynamic test rig. (a) Major components and instrumentation, (b) Hot cartridge heater at 360ºC and rotor spinning at 30 krpm.

(a) Front view   (b) Oblique view

(c) Zoomed view "A"
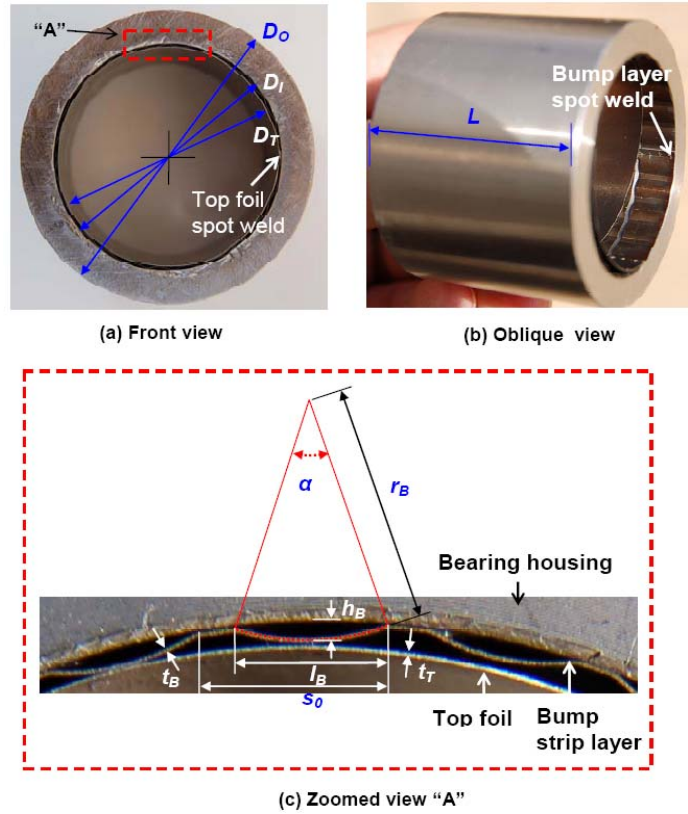
Fig. 2 Photograph of 2nd generation bump type test GFB with uncoated top foil and its dimensions. Taken from Ref. [13]

Table 1. Test foil bearing nominal dimensions (Unit: mm) [13]

Parameters	Drive end (DE) GFB	Free end (FE) GFB
Bearing cartridge outer diameter, D_O	50.85	50.82
Bearing cartridge wall thickness, t_{BC}	5.746	5.776
Bearing cartridge inner diameter, $D_I = D_O - 2\,t_{BC}$	39.36	39.27
Bearing axial length, L	38.2	38.14
(bare top foil) Top foil thickness, t_T	0.10	0.10
Bump foil thickness, t_B	0.10	0.10
Number of Bumps, N_B	25	25
Bump pitch, s_0 (deg)	4.581 (13)	4.581 (13)
Bump length, l_B	3.742	3.742
Bump height, h_B	0.468	0.468
Bump arc radius, r_B	5.581	5.581
Bump arc angle, α (deg)	36.5	36.5
Top foil inner diameter, $D_T = D_I - 2(t_T + h_B)$.	38.190	38.135
Poisson's Ratio	0.29	0.29
Modulus of Elasticity (GPa)	213736	213736

1) Manufacturer: Foster-Miller Technologies
2) Material: Cr-Mb steel (bump strip and top foil), AISI 304 stainless steel (bearing cartridge)

Infrared thermometers measure the rotor surface temperatures at each end of the test rotor. The uncertainty and response time of the transmitter are 1.7°C (3°F) and 250 ms, respectively. Note that the sensor has an adjustable emissivity setting.

Two pairs of eddy current sensors (Bently Nevada 7200 Series), orthogonally positioned and facing the rotor ends, measure lateral displacements of the test rotor along the vertical and horizontal planes. Table 2 shows the calibrated sensitivity of the eddy current sensors installed. An infrared tachometer, mounted on the test table and targeting one end of the flexible coupling, is a keyphasor signal for data acquisition.

Table 2 List of sensors gains

Name	Location	Sensitivity	Unit
	Drive end, vertical direction (DV)	7.97	mV/μm
Displacement eddy current sensors	Drive end, horizontal direction (DH)	8.31	mV/μm
	Free end, vertical direction (FV)	8.04	mV/μm
	Free end, horizontal direction (FH)	8.06	mV/μm

Commercial DAQ systems (*Bentley Nevada ADRE® for Windows* and *LabVIEW®*) collect and record the test data from coast down rotor speed experiments. Table 2 shows the sampling size and acquisition rate of the *ADRE®* DAQ system.. The sampling size and rate for *LabVIEW®* are 2048 (2^{11}) and 10,000 samples/sec, respectively. A custom *LabVIEW®* graphical user interface (GUI) shows both time domain and frequency-domain representations of each signal during real time monitoring and data logging. A two-channel dynamic signal analyzer displays the frequency content of selected motion signals.

Appendix B details the components of the test rig, including commercial designations, their cost and assigned source for payment.

Experimental Procedure

Figure 3 shows a schematic view of the high temperature GFB rotordynamic test rig with the cartridge heater and temperature measurement locations of the test rig components: $T_1 \sim T_{16}$, T_{amb} and T_h. Recall that the electric heater is inserted loosely into the hollow portion of the shaft. The radial gap between these two components is 4.75mm.
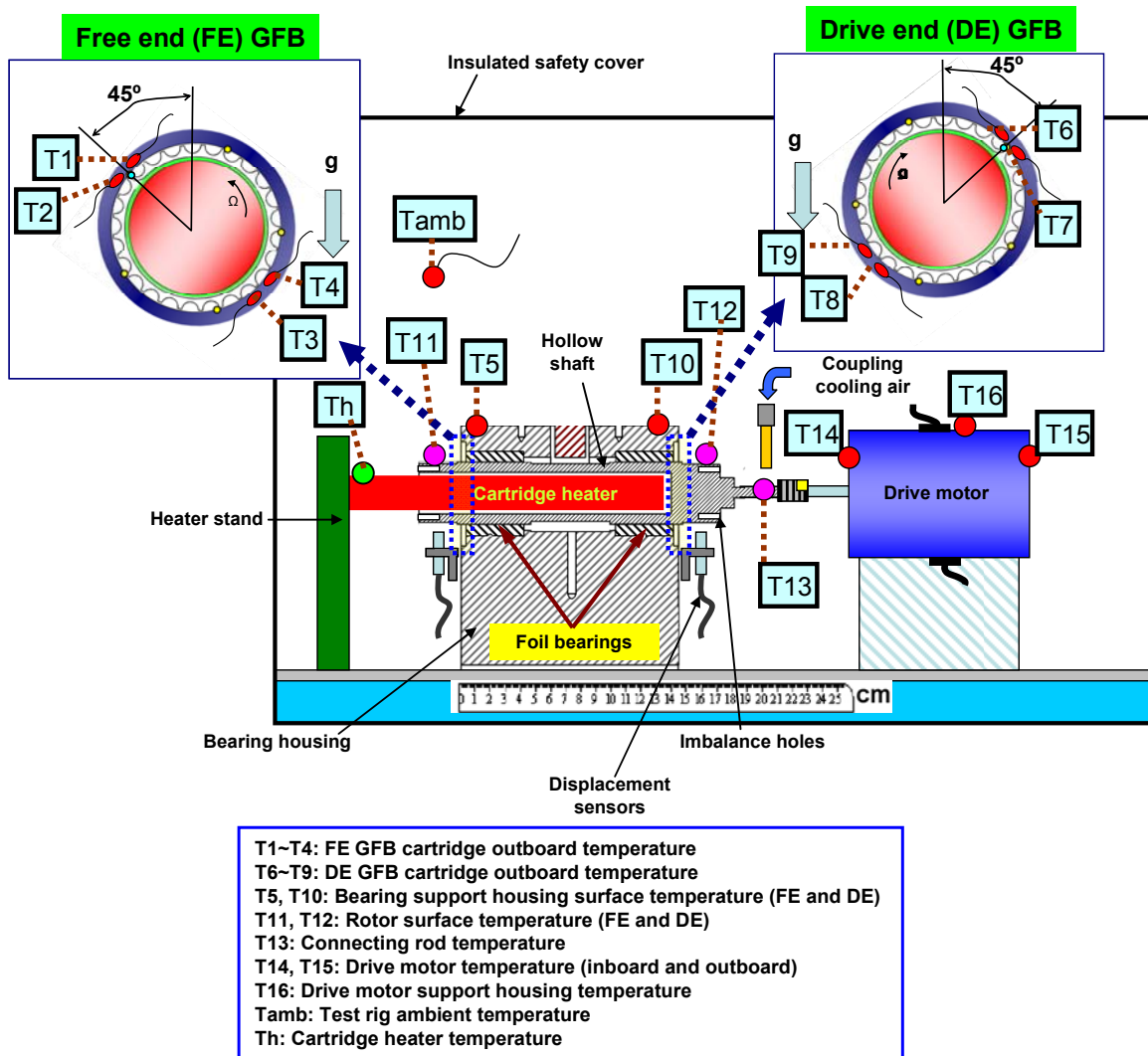
Fig. 3 Schematic view of GFB rotordynamic test rig with cartridge heater. $T_1 \sim T_{16}$, T_{amb}, T_h **represent locations of temperature measurement.**

Table 3 presents the matrix of test conditions for increasing heater set temperatures (T_{hs}=100°, 200°, 300°, and 360°C), without and with increasing axial cooling air flow rates (100, 200, and 300 L/min). Note that the flow rates quoted distribute (evenly) into the two bearings, drive end (DE) and free end (FE), thereby supplying 50, 100, and 150 L/min per each bearing.

Table 3 also lists the time elapsed for the (whole) test rig to reach thermal equilibrium, i.e. temperatures in the components not changing any longer with time (steady state). For test conditions 4 through 12, the sides of the (insulating) enclosure remain open to reduce the operating time for thermal equilibrium condition of the test system and to minimize thermal induced damage of the instrumentation and drive motor.

Table 3 Matrix of experimental test conditions in high temperature GFB rotordynamic test rig[4]

Test condition #		Rotor speed condition	Imbalance conditions	Axial cooling flow conditions*	Heater set temperature conditions	Test hours	Rig enclosure
Cond. 1	Rotor imbalance response measurement test (**Room temperature**)	Fixed speed of 0, 10, 15, 20, 25, 30 krpm	Baseline	No cooling	No heating	9h 9'	Closed
Cond. 2				100L/min		5h 52'	
Cond. 3		Coast down from 30 krpm	Baseline	No cooling		5 '	
			60mg in phase				
			110mg in phase				
			184mg in phase				
Cond. 4	Rotor imbalance response test (**High temperature**)	Coast down from 30 krpm	Baseline	No cooling	No heating	1h 15'	Open
					100ºC	1h 37'	
					200ºC	1h 40'	
					300ºC	1h 32'	
					360ºC	1h 35'	
Cond. 5			60mg in phase		No heating	1h 37'	
					100ºC	1h 41'	
					200ºC	1h 24'	
					300ºC	1h 21'	
					360ºC	1h 30'	
Cond. 6			110mg in phase		No heating	1h 38'	
					100ºC	1h 48'	
					200ºC	1h 40'	
					300ºC	1h 50'	
					360ºC	1h 41'	
Cond. 7	Temperature measurement for **increasing rotor speed**	Fixed rotor speed of 10, 20, 30 krpm	Baseline	No cooling	No heating	1h	
Cond. 8				100L/min			
Cond. 9	Temperature measurement for **increasing heater temperature**	Fixed rotor speed of 30 krpm	Baseline	No cooling	No heating, 100, 200 300, 360ºC		
Cond. 10				100L/min			
Cond. 11				200L/min	No heating, 100, 200 ºC		
Cond. 12				300L/min	No heating, 100, 165ºC		

(*) Total flow splits in ½ into each foil bearing

In the experiments, the rotor speed reaches a maximum of 30 krpm. Over the speed range (2-30 krpm), the test rotor is not regarded as a rigid body. Details on the natural frequencies and mode shapes of the test rotor-bearing system follow later.

For **test conditions 3, 5 and 6,** added masses (m_i) are inserted in the holes located at the rotor ends and at a radial distance (r) of 15.11 mm. The imbalance displacement (u), i.e. distance from rotor center of mass, is

$$u = \frac{m_i r}{m_i + M_{DE\ or\ FE}} \tag{1}$$

where M_{DE} and M_{FE} are fractions of the test rotor weight acting on each bearing: M_{DE} =0.698 kg (6.844 N) and M_{FE} =0.366 kg (3.589 N), respectively[5]. Table 4 shows the imbalance mass

---

[4] Prior to each test condition, the whole rotor-bearing system is at room temperature, i.e., the drive motor and cartridge heater are turned off for ~ 24 hours.
[5] The force acting on the flexible coupling is not considered for the static load distribution.

and its location, as well as the displacements u for each condition. The imbalance masses are positioned at the same angular location at each rotor end, i.e., in phase imbalance condition.

Table 4. Imbalance mass magnitudes and location

Imbalance name	Mass m_i (g)[6]		Displacement u (μm)	
(In phase)	Drive end (-22º)	Free end (-22º)	Drive end	Free end
U_1	0.060	0.060	1.30	2.48
U_2	0.110	0.110	2.38	4.54
U_3	0.184	0.184	3.98	7.60

Over the whole set of test conditions, while the rotor operates, a stream of compressed shop air (20 psig, 23ºC) cools the flexible coupling[7] through a plastic hose and nozzle. In the following, the designations DV and DH correspond to the rotor responses at the drive end bearing side, vertical and horizontal plane, respectively. The same notation follows for the free end bearing, FV and FH.

Experimental Results

Verification of rotor-bearing system response linearity: Test condition 3.

Test condition # 3	Rotor speed condition	Imbalance conditions	Axial cooling flow conditions	Heater set temperature conditions	Test time	Rig enclosure
Rotor imbalance response measurement test (**Room temperature**)	Coast down from 30 krpm	Baseline	No cooling	No heating	5'	Closed

For test condition 3 (without heating and forced cooling), rotor speed coast down measurements from 30 krpm are conducted with the rotor at its baseline condition and with added imbalance masses. Figure 4 shows the normalized rotor amplitudes of the measured synchronous responses. In the figures, the baseline response is subtracted (amplitude and phase) from the measured imbalance response and normalized by multiplying the ratio of the added mass $U_{2\text{ or }3}/U_1$. In this manner, the linearity of the test rotor-GFBs system response can be easily verified.

---

[6] Uncertainty in mass is ±0.001g
[7] The flexible coupling consists of a steel bellow and aluminum clamping hubs. The coefficient of thermal expansion of aluminum (coupling clamp hub material) and Inconel 718 (rotor material) are 24.0 μm/m°C and 13.0 μm/m°C, respectively [18]. Hence, temperature management of the coupling is mandatory for high temperature operation.

The three response curves in Figure 4 are nearly identical, thus denoting the rotor amplitude of synchronous response is proportional to the added mass imbalance. This implies that a rotordynamic model that integrates linearized GFB force coefficients will predict the rotor behavior correctly. The speeds at which discernible rotor response amplitude peaks at the DH and FH are 13.4 krpm and 12 kprm, respectively.
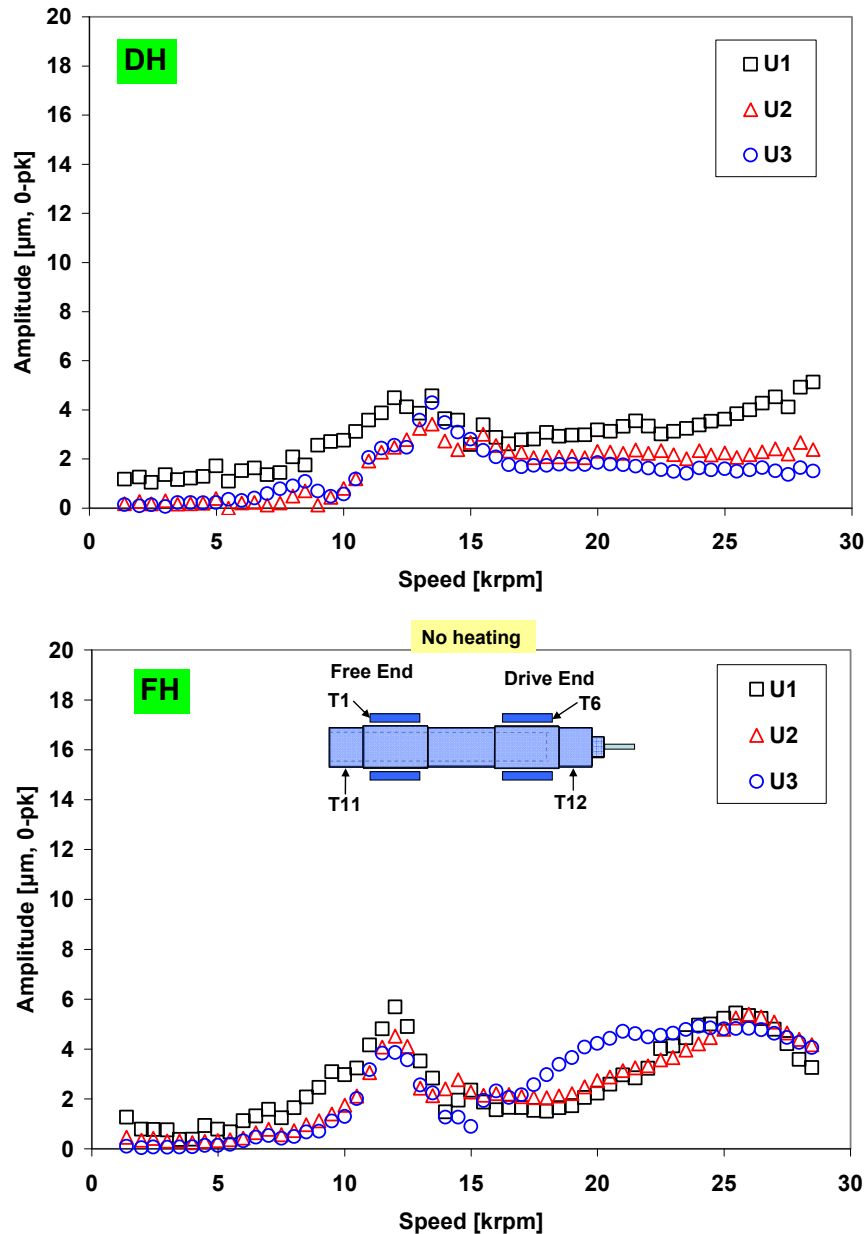
Fig. 4 Test condition 3: Normalized amplitude of synchronous response for in-phase imbalance masses of 60mg (U1), 110mg (U2), and 184mg (U3). Measurements at rotor drive end horizontal (DH) and rotor free end horizontal (FH) planes with baseline subtraction.

Test condition #		Rotor speed condition	Imbalance conditions	Axial cooling flow conditions	Heater set temperature conditions	Test hours	Rig enclosure
Cond. 4	Rotor imbalance response test (**High temperature**)	Coast down from 30 krpm	Baseline	No cooling	No heating	1h 15'	Open
					100ºC	1h 37'	
					200ºC	1h 40'	
					300ºC	1h 32'	
					360ºC	1h 35'	
Cond. 5	Rotor imbalance response test (**High temperature**)	Coast down from 30 krpm	60mg in phase	No cooling	No heating	1h 37'	
					100ºC	1h 41'	
					200ºC	1h 24'	
					300ºC	1h 21'	
					360ºC	1h 30'	
Cond. 6	Rotor imbalance response test (**High temperature**)	Coast down from 30 krpm	110mg in phase	No cooling	No heating	1h 38'	
					100ºC	1h 48'	
					200ºC	1h 40'	
					300ºC	1h 50'	
					360ºC	1h 41'	

For test condition 4, Fig. 5 depicts the recorded amplitudes of synchronous rotor response during a rotor speed coastdown test from 30 krpm. Slow roll compensation is at 2 krpm[8]. This response is regarded as baseline since it does not include any added imbalance mass. The rotor amplitudes are well damped at speeds around the system first critical speed region (11~13 krpm), gradually increasing as the rotor speed approaches 30 krpm. Rap tests demonstrate the flexible mode natural frequency of the test system at 29 krpm (480 Hz). Multiple peaks in rotor synchronous responses are evident and reveal the different forced response characteristics along the vertical and horizontal directions. There are no noticeable differences in rotor responses for both the shaft without heating and with heater at T_{hs}=360ºC conditions. The figures show insets denoting the measured rotor end temperatures. Note in particular the large axial thermal gradient (~50ºC) for the hot rotor condition.

---

[8] The slow roll speed is typically less than 10% of the full operating speed of the rotor [19].

(a) No heating

Heater temperature increases
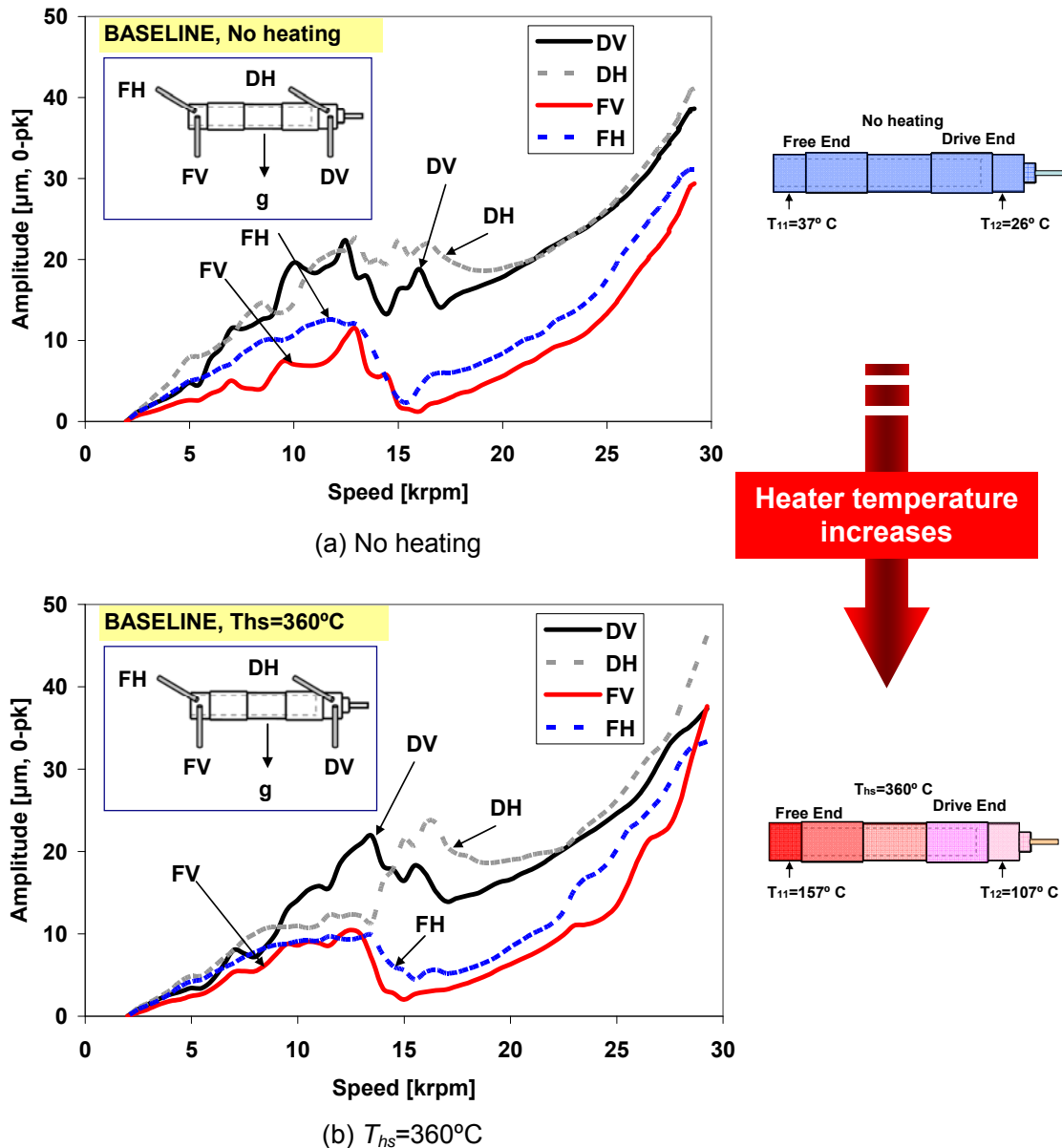
(b) T_{hs}=360°C

Fig. 5 Test condition 4: Amplitude of rotor synchronous response versus rotor speed. Slow roll compensation at 2 krpm. No axial cooling flow into bearings. Baseline imbalance. Tests at room temperature and with heater at T_{hs}=360°C.

The mode shape of the rotor response can be readily determined by subtracting the phase angles of the measure motions at the drive and free end of the rotor. Note that the rotor is <u>rigid</u> at low speeds, below 15 krpm. On the other hand, as the speed increases beyond 20 krpm, the rotor shows a distinctive <u>flexural</u> mode due to the softness of the coupling and connecting rod. For test condition 4 (without shaft heating), Fig. 6 depicts the phase angle difference ($\angle$ FH - $\angle$ DH) ~180° denoting a conical mode at speeds around the system first critical speed range, 11~13 krpm. Note that this phase difference abruptly drops at ~15 krpm

and ranges between 110º and 180º at 15~10 krpm. The figure also displays the ratio of amplitudes (drive end/free end) of the rotor. This ratio determines the relative amplitude of the major amplitude rotor (end) motion at the measurement locations. The rotor moves in a conical mode shape at speeds below 13 krpm. In particular, when the rotor operates between 15 and 20 krpm, the overall amplitude of rotor motion at the drive end rotor is 2~9 times larger than those at free end rotor.
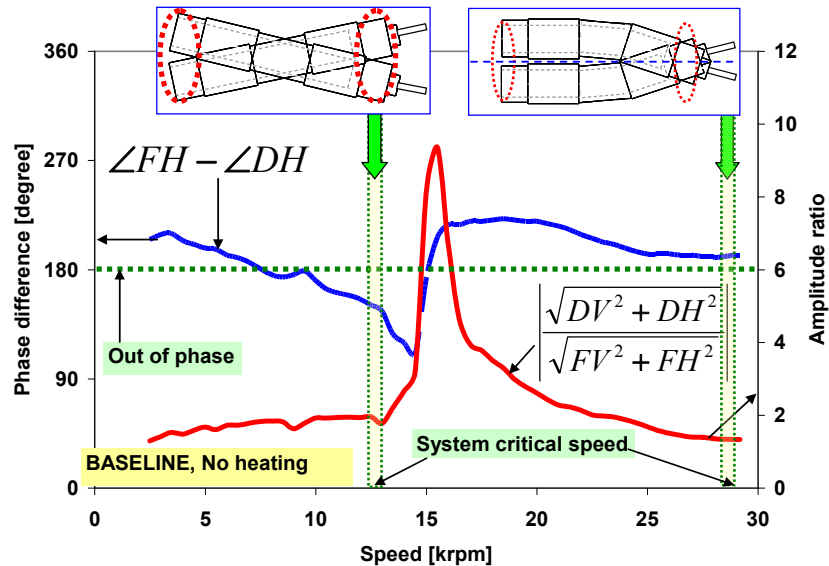
Fig. 6 Test condition 4: Phase difference ($\angle FH - \angle DH$) and major amplitude ratio ($\left| \sqrt{DV^2 + DH^2} / \sqrt{FV^2 + FH^2} \right|$) of recorded imbalance response. No rotor heating. No axial cooling flow into bearings. Baseline imbalance.

For operation at four heater set temperatures (T_{hs}=100º, 200º, 300º, 360ºC) and also while at room temperature (heater off), equivalent to test condition 4, Fig. 7 depicts the synchronous rotor amplitude and lag phase angles recorded during rotor speed coastdown tests. Recall that no cooling flow is supplied. In general, as T_{hs} increases to 360ºC, the peak amplitudes[9] between 7~15 krpm decrease significantly. The phase angles, over the whole speed range, slightly decrease with increasing heater temperatures. Recall that thermally induced mechanical changes in the shaft and bearing can noticeably affect the operating clearance and gas film properties in GFBs [11]. Note the phase angle ranges 0~360º since the test rotor-bearing system crosses two natural modes, rigid and flexural. The figure shows insets denoting the measured rotor end temperatures.

---

[9] Note that the displacement peak amplitude is not evident (multiple peaks as well as a too broad band due to high damping) to identify a *true* system critical speed.
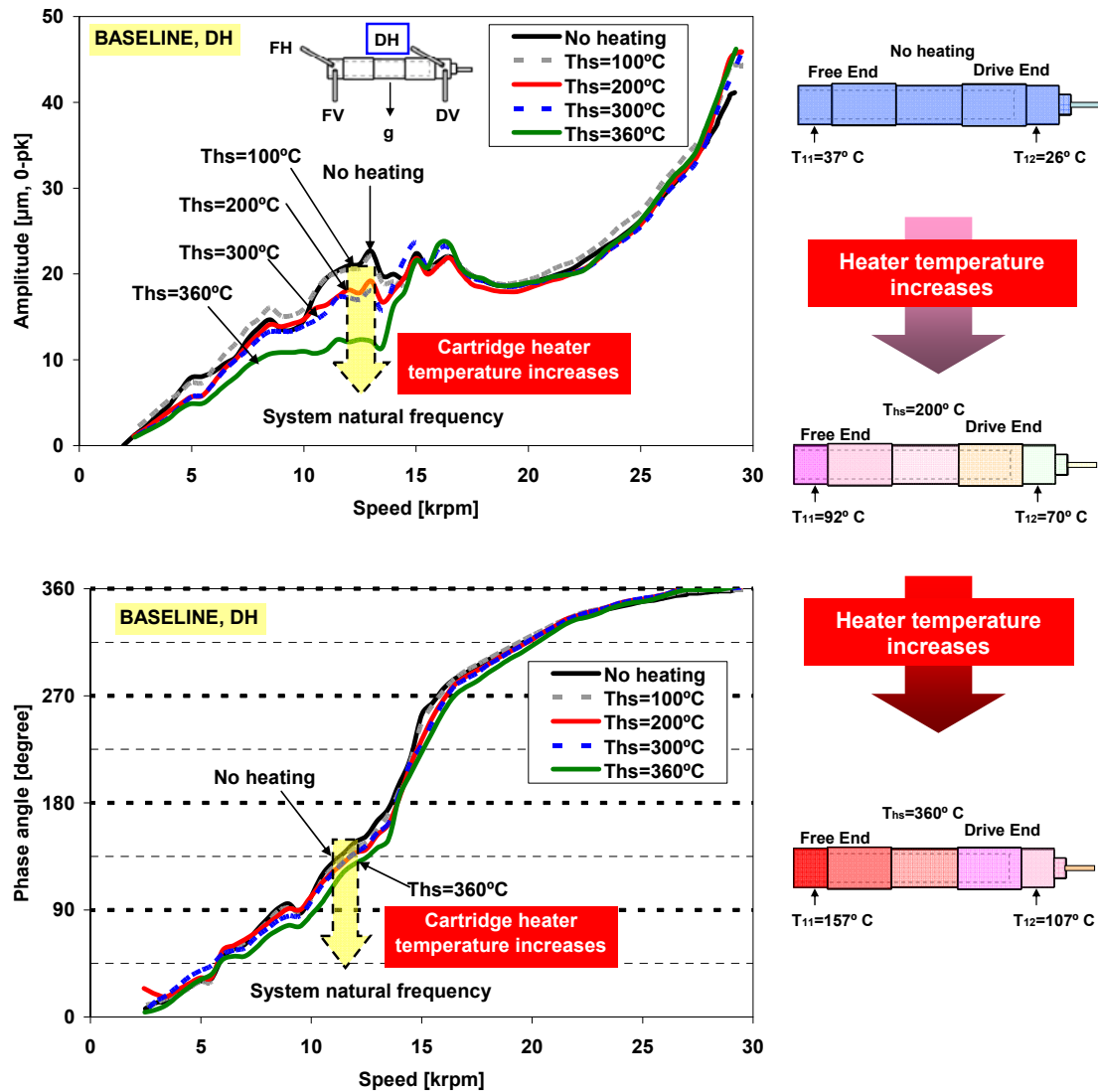
Fig. 7 Test condition 4. Effect of shaft temperature on rotor response: Rotor amplitude and lag phase angle of synchronous response for four cartridge heater set temperatures (T_{hs}). No axial cooling flow into bearings. Slow roll compensation at 2 krpm. Baseline imbalance. Rotor drive end, horizontal plane (DH).

Figure 8 shows waterfall plots depicting the amplitude and frequency contents (1X and 2X) of the rotor motions as the rotor coast downs from 30 krpm. The measurement corresponds to test condition 4, i.e., baseline without axial forced cooling into the bearings. Note that, for all test conditions, no subsynchronous whirl motions appear over the whole speed range. From the top speed to ~16 krpm, there is dominance of synchronous rotor motions and small amplitude super-synchronous frequencies (2X and 3X).

(a) No heating

(b) T_{hs}=360ºC
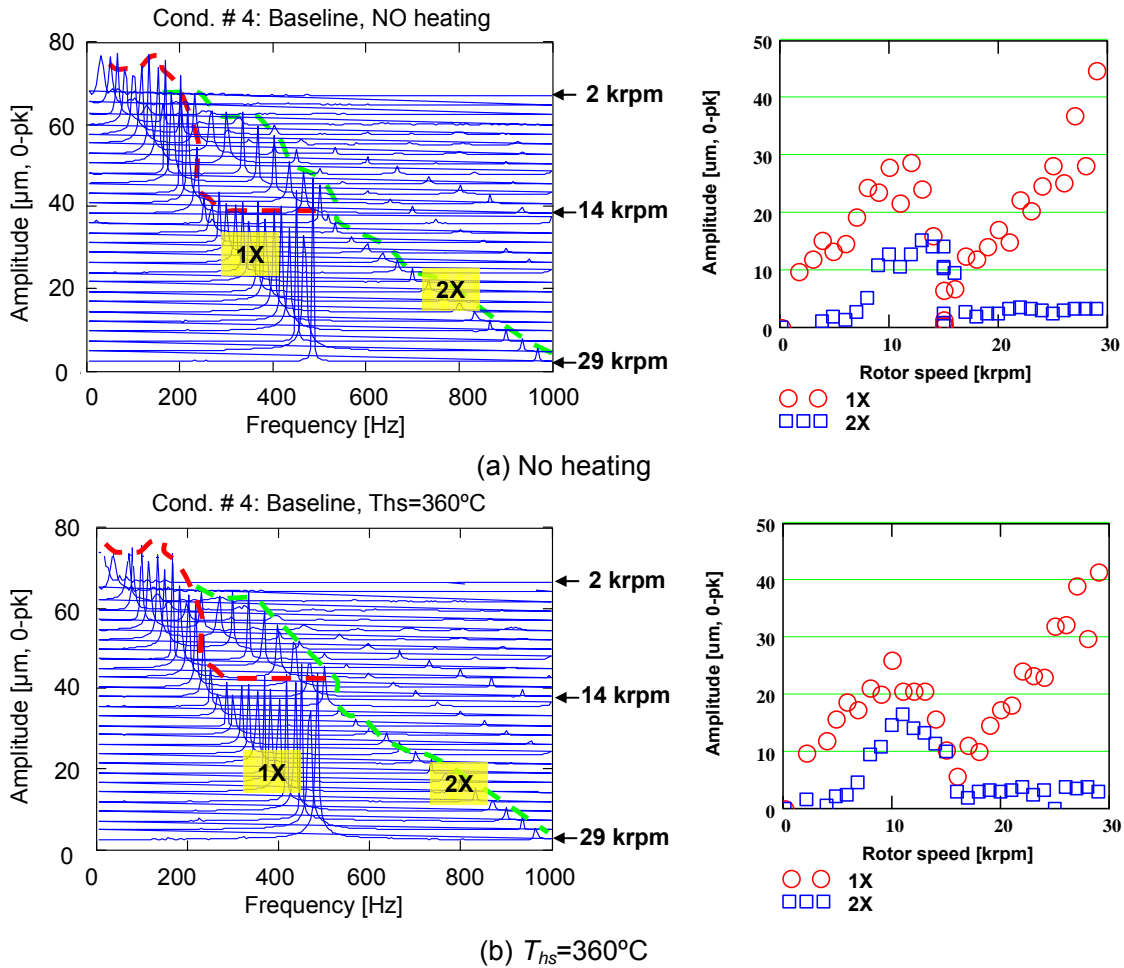
Fig. 8 Test condition 4: **Waterfalls and amplitude of synchronous (1X) and 2X rotor motions. Uncompensated amplitudes of motion. Rotor drive end, horizontal plane (DH). Tests w/o heating and with heating at** T_{hs}**=360ºC**

    Figure 9 shows the synchronous (1X) rotor orbits at rotor speeds equal to 5, 10, 15, 20 krpm for test condition 4 (no axial cooling streams). Recall that the orbit represents the path of the shaft centerline relative to a pair of orthogonally mounted displacement sensors [20]. In the figure, the blank/dot sequence on each orbit represents a keyphasor mark which shows the location of the shaft centerline at the instant when the reflective mark (once-per-revolution mark) passes the keyphasor probe (tachometer). The keyphasor mark in an orbit curve aids to determine the instantaneous direction of rotor motion (CCW direction in Fig. 9) and to estimate the absolute phase; and with multiple orbit plots, the mode shape of the rotor [21]. Note that the orbits w/o heating and with heater at T_{hs}=360ºC are almost identical at similar shaft speeds. The ellipticity of the orbital motion shows the anisotropic character of the foil bearing stiffnesses. The 1X orbits are nearly circular at rotor speed above 20 krpm.

Note the keyphasor marks imply out of phase motions between the drive end and free end of the rotor over the entire speed range.

(a) No heating

(b) T_{hs}=360ºC
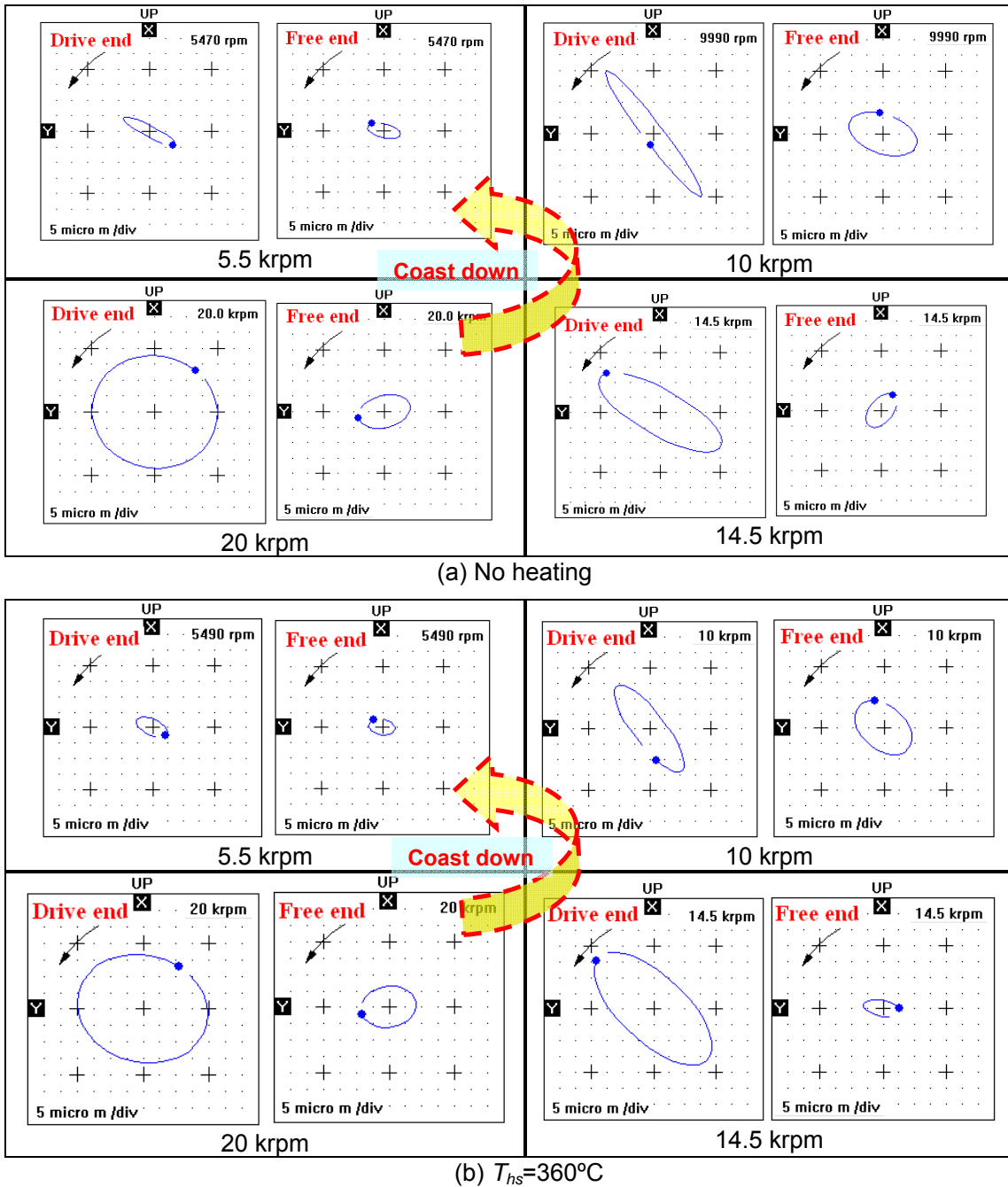
Fig. 9 Test condition 4: Synchronous speed rotor orbits. (a) no heating (heater off), and (b) heater at T_{hs}=360ºC. Slow roll compensated at 2 krpm.

While coasting down from a top speed of 30 krpm to rest, Fig. 10 depicts the recorded coastdown rotor speed versus time at increasing heater temperatures for test condition 4. The time for the rotor to coast down is over 50 seconds which denotes very low air drag operation

(nearly friction free). The results reveal an exponential decay of rotor speed with time for speeds from 30 krpm to ~11 krpm. Then, the rotor rapidly decelerates to rest, thereby evidencing rubbing (dry friction effects) in the rotor-bearing operation. The calculated (correlation coefficient) R^2 of both exponential and linear decays in the figure renders a goodness of correlation of 99%. Exponential decay in a speed coastdown curve is typical of a rotating system with viscous drag, and hence demonstrates no contact between the rotor and the bearing surfaces. For speeds below ~11 krpm, the rotor speed decays nearly linearly, typical of mixed drag conditions, i.e., viscous and with dry-friction. The overall coast down time reduces noticeably as the rotor becomes hot. For example, the overall coast down time for T_{hs}=360ºC is ~10 second shorter than that for the *no heating* (heater off) tests (16% decrease in overall coastdown time). As the rotor temperature increase, the rotor touchdown speed (transition from viscous drag to dry friction) also decreases.
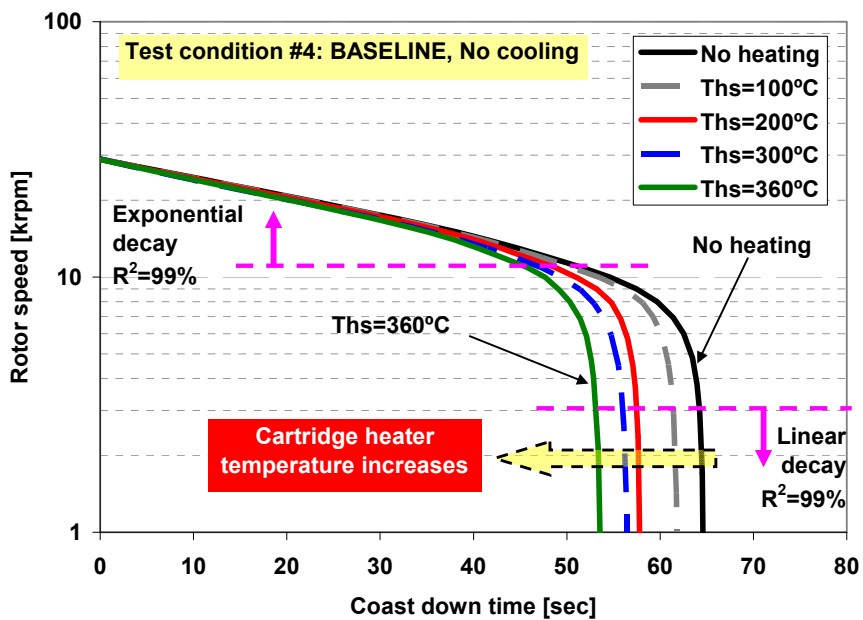
Fig. 10 Test condition 4. Effect of shaft temperature on time extent for speed coastdown: Tests with increasing heater temperatures. Baseline imbalance.

Test condition #		Rotor speed condition	Imbalance conditions	Axial cooling flow conditions	Heater set temperature conditions	Test hours	Rig enclosure
Cond. 7	Temperature measurement for **increasing rotor speed**	Fixed rotor speed of 10, 20, 29.3 krpm	Baseline	No cooling	No heating	1 h	Open
Cond. 8				100L/min			

In test conditions 7 and 8 (with electrical heater off), the bearing and rotor temperatures are recorded while the rotor operates at a constant speed (10, 20 and 30 krpm). The tests correspond to conditions without and with forced axial cooling flow (50 L/min per bearing). The ambient temperature is $T_a \sim 21\,°\text{C}$.

In the tests, after 20 minute intervals, the rotor speed is set at 10 krpm, then at 20 krpm, and finally at 29.3 krpm. The temperatures shown below represent thermal steady state conditions. The total experiment lasts 60 minutes (1 hour). Figure 11 shows the temperature raise of the free end (FE) and drive end (DE) rotor surfaces (T_{11} and T_{12}) and the FE and DE bearing cartridges (T_1 and T_6) versus test elapsed time. See Fig. 3 for designation of thermocouples. The recorded bearing cartridge and rotor surface temperatures steadily increase with operating time. For operation without or with 50 L/min axial cooling, the temperatures of the FE and DE bearing cartridges (T_1 and T_6) are almost identical. Note that the free end rotor surface (T_{11}) shows the largest temperature raise as operation time and rotor speed increase.

Fig. 11 Test conditions 7 and 8: Temperature raises in FE and DE FB cartridges, T_1-T_{amb} and T_6-T_{amb}, and FE and DE shaft surface, T_{11}-T_{amb} and T_{12}-T_{amb}, versus rotor speed. Operation at <u>ambient condition</u>, T_{amb} =21ºC. Without and with 50 L/min cooling stream into each bearing.

Figure 12 shows the temperature raise on the FE and DE GFB cartridges, (T_1-T_{amb}) and (T_6-T_{amb}), versus rotor speed. See Fig. 3 for the locations of the thermocouples. The bearing cartridge and rotor surface temperatures increase as the rotor speed increases. The forced axial cooling flow produces an effective decrease in bearing temperatures. At 29.3 krpm, the bearing cartridge temperature with 50 LPM cooling reduces the overall temperature as much as 5ºC (a drop of 44% in temperature raise when compared to the no cooling condition). Note, however, the insignificant effect of cooling flow on the rotor surface temperature, irrespective of shaft speed (only ~1ºC decrease). The paramount effect of the cooling flow stream in the bearings is distinct at the highest rotor speed, ~30 krpm. More discussion of the effect of forced axial cooling follows later.

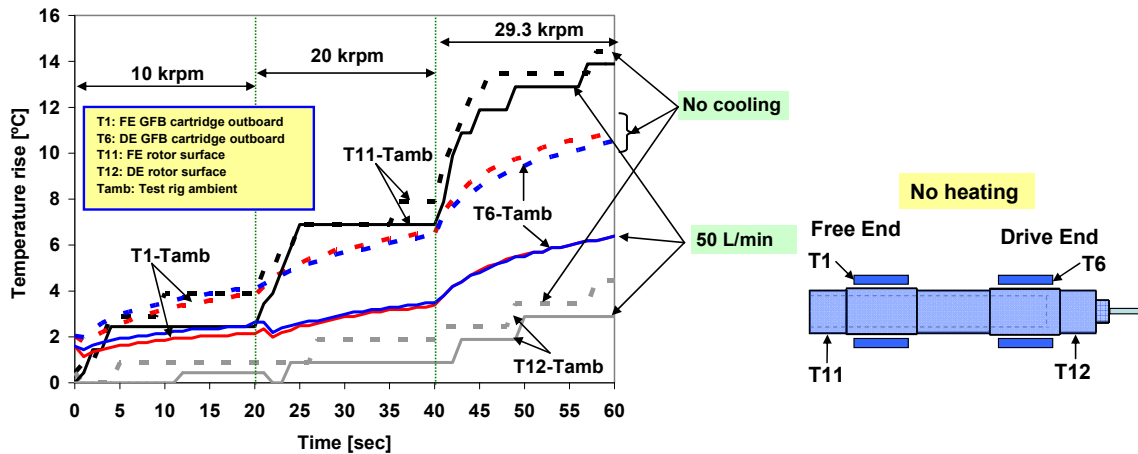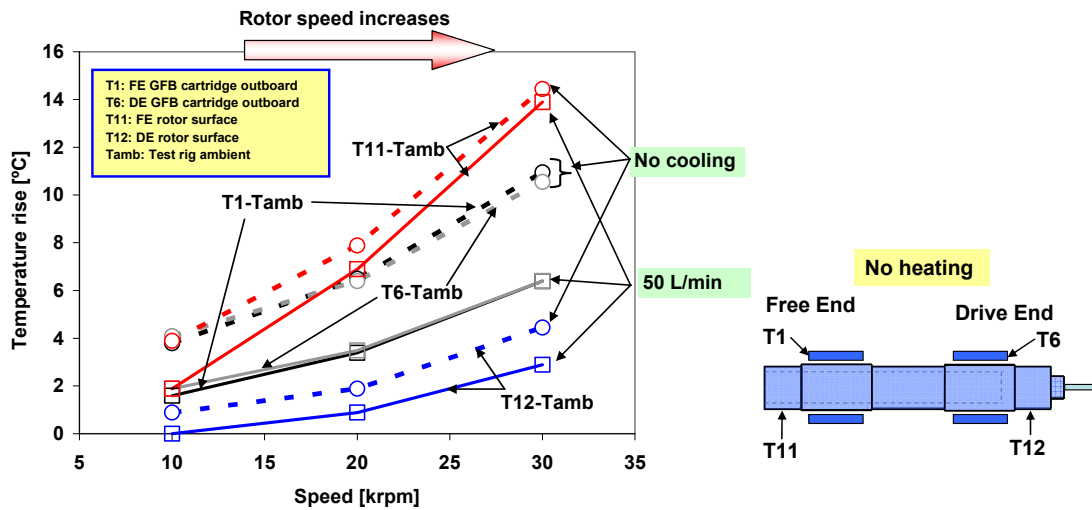**Fig. 12 Test conditions 7 and 8. Effect of rotor speed on bearing temperature raise: Temperature raise in FE and DE FB cartridges, T_1-T_{amb} and T_6-T_{amb}, and FE and DE shaft surface, T_{11}-T_{amb} and T_{12}-T_{amb}, versus rotor speed. Operation at _ambient condition_, T_{amb}=21ºC. With 50 L/min and without cooling stream to each bearing.**

Test condition #		Rotor speed condition	Imbalance conditions	Axial cooling flow conditions	Heater set temperature conditions	Test hours	Rig enclosure
Cond. 9	Temperature measurement for **increasing heater temperature**	Fixed rotor speed 29.3 krpm	Baseline	No cooling	No heating, 100, 200, 300, 360ºC	1 h	Open
Cond. 10				100L/min			
Cond. 11		Fixed rotor speed 29.3 krpm		200L/min	No heating, 100, 200 ºC		
Cond. 12				300L/min	No heating, 100, 165ºC		

For test condition 9 (without forced cooling), Fig. 13 shows the temperatures raise of the cartridge heater ($T_h - T_{amb}$), the free end (FE) and drive end (DE) rotor surfaces, ($T_{11} - T_{amb}$ and $T_{12} - T_{amb}$), and the FE and DE bearing cartridges, ($T_1 - T_{amb}$ & $T_6 - T_{amb}$), versus elapsed test time. After a 20 minute interval, in similar fashion as in test conditions 7 and 8, the cartridge heater temperature (T_{hs}) is set at 100 ºC, 200 ºC, 300 ºC and 360ºC[10]. The rotor speed is 29.3 krpm.

Recall that the heater cartridge does not heat evenly the hollow rotor. There is an axial thermal gradient from the rotor free end towards its drive end. The measurements show that the rotor, although much cooler than the heater, has a temperature path which parallels that of the heater. The temperatures on the bearing cartridges, on the other hand, increase steadily with time.
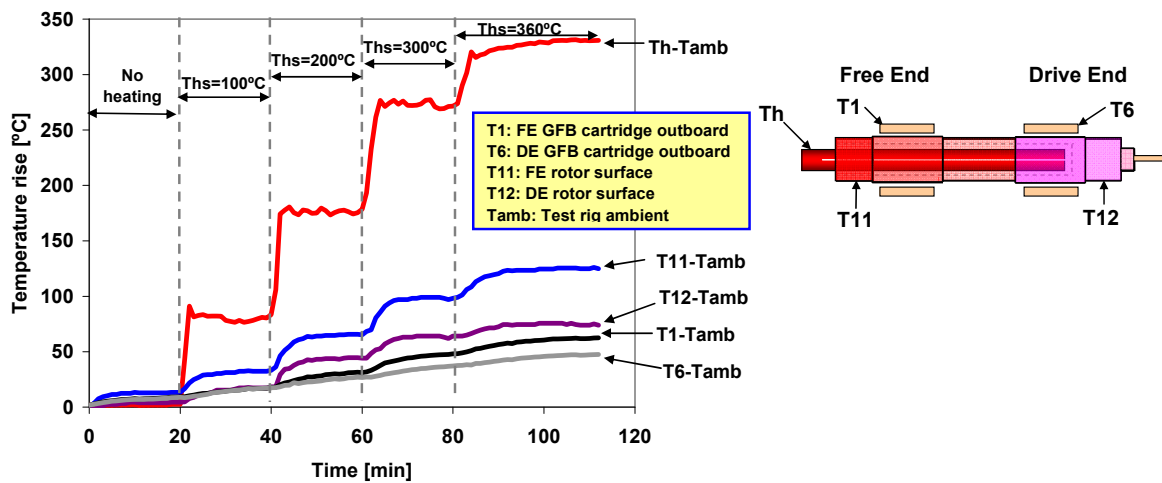
Fig. 13 Test condition 9: Recorded temperature raises of cartridge heater (T_h - T_{amb}), rotor free end (FE): (T_{11} - T_{amb}) and drive end (DE): (T_{12} - T_{amb}), and FE and DE bearing cartridges (T_1 - T_{amb} & T_6 - T_{amb}). Heater set temperature (T_{hs}) at 100 ºC, 200 ºC, 300 ºC, and 360ºC. Rotor speed = 29.3 krpm. No cooling flow into bearings. Baseline condition.

For test conditions 9 through 12, i.e. with increasing strength of the cooling gas stream (0 – 150 L/min per bearing), Fig. 14 depicts the measured heater temperature (T_h) and the temperature raise on the FE and DE GFB cartridges, (T_1-T_{amb}) and (T_6-T_{amb}), versus elapsed test time. Note that the maximum operating temperature of the cartridge heater surface reduces from 360ºC (without cooling and with 50 L/min per bearing) to 190ºC and 165ºC for 100 L/min and 150 L/min cooling flows, respectively. Since the heater electrical power is limited, the reduction in its surface temperature is due to the cooling flow with increasing strength quickly advecting heat from the whole test rig. The measurements show that without a forced cooling flow the temperature raise in the bearing cartridges is highest. The effectiveness of the cooling method is clearly demonstrated for flows above 100 L/min. Note that at highest heater temperature, the effect of cooling flow is most distinctive.

At T_{hs}=360ºC, the recorded maximum cooling capability of the forced axial flow on the FE bearing cartridge temperature is 0.44ºC/LPM (22ºC decrease due to 50 L/min at 30 krpm). Note that, for operation at ambient or a lower heater temperature condition, the cooling flow stream demonstrates very limited effectiveness, for example, 0.05 ºC/LPM (5 ºC decrease due to 100 L/min at 30 krpm) and 0.09 ºC/LPM (9 ºC decrease due to 100 L/min at 30 krpm) for no heating and T_{hs}=100ºC, respectively.

---

[10] Maximum operating temperature of the cartridge heater (rated at 400W with 120VAC) is 360ºC while the rotor operates at a speed of 30 krpm and without cooling flow into the test bearings.

(a) Cartridge heater temperature (T_h)

T1: FE GFB cartridge outboard
T6: DE GFB cartridge outboard

(b) Temperature raise (T_1-T_{amb}) and (T_6-T_{amb}) in foil bearing cartridges
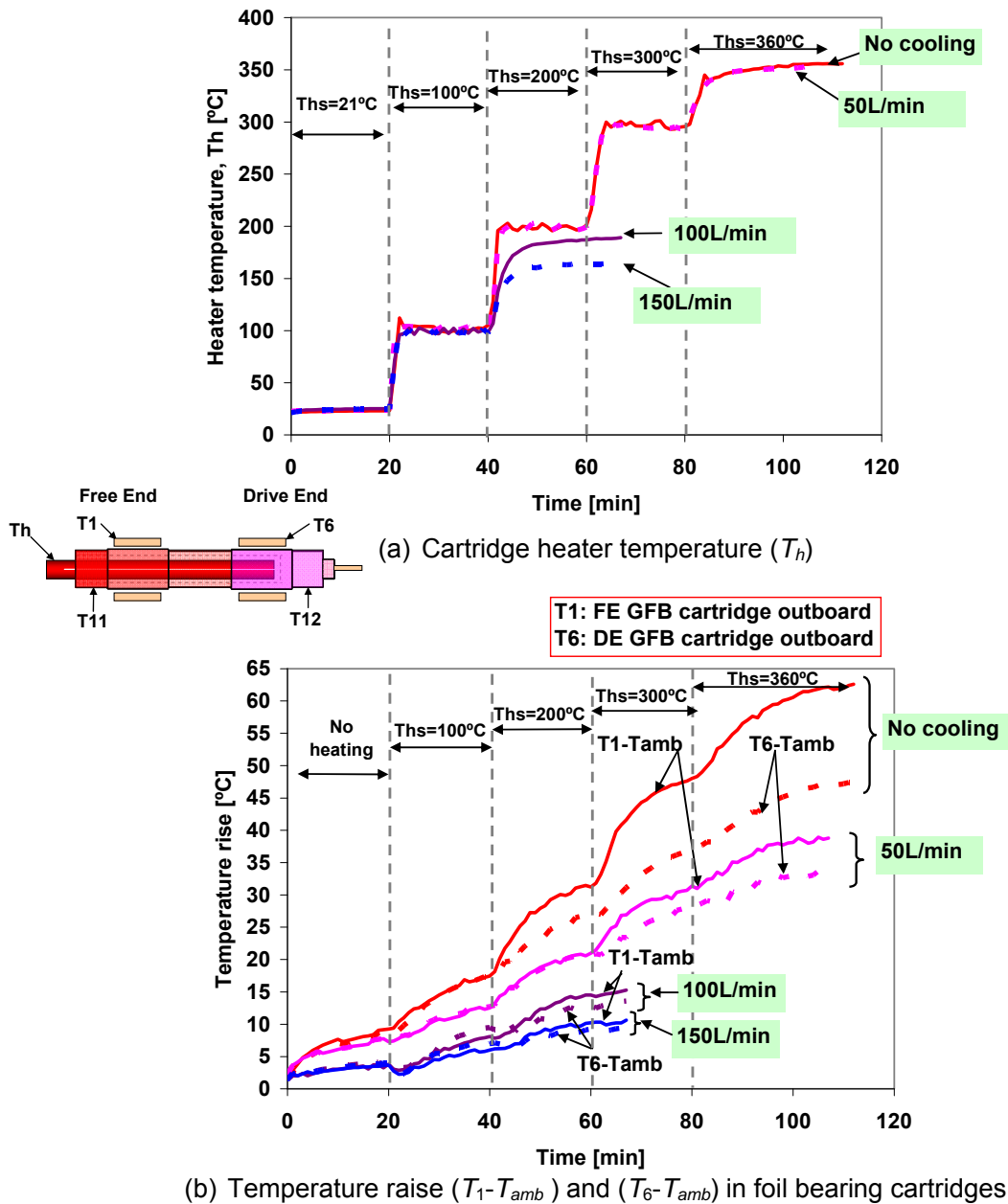
Fig. 14 Test conditions 9-12: (a) Cartridge heater temperature (T_h) and (b) temperature raises in FE and DE FB cartridges, (T_1-T_{amb}) and (T_6-T_{amb}), versus elapsed time for increasing strengths of cooling stream (max. 300L/min). Heater set temperature (T_{hs}) at 100 ºC, 200 ºC, 300 ºC and 360ºC. Rotor speed of 29.3 krpm.

For two set heater temperatures, 100 ºC and 200 ºC, Fig. 15 depicts the temperature raise on the FE and DE GFB cartridges, (T_1-T_{amb}) and (T_6-T_{amb}), quickly decreasing with the strength of the cooling flow rate. The measurements show that the lowest flow rate (50 LPM) produces the largest thermal gradient, i.e. the largest difference in bearing operating temperatures. The largest cooling stream (150 LPM) hardly changes the bearing temperatures

when compared to the results produced by a weaker one, i.e. 100 LPM. It is presumed that flow rates >100 LPM are already turbulent in character.
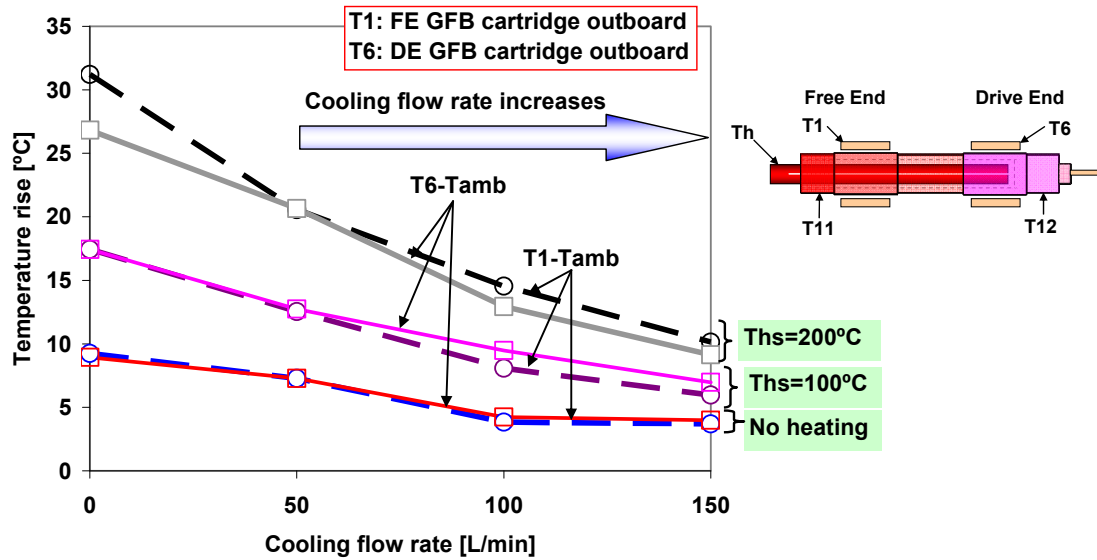
Fig. 15 Test conditions 9-12. Effect of cooling flow on bearing temperatures: **Temperature raise in FE and DE FB cartridges, (T_1-T_{amb}) and (T_6-T_{amb}), versus strength of cooling flow stream. Operation at ambient condition and with cartridge heater set temperature (T_{hs}) at 100, 200ºC. Rotor speed of 29.3 krpm.**

Figure 16 depicts the recorded rotor speed coastdown versus time without and with 50 LPM/bearing axial cooling (corresponding to test conditions 7 through 10). For operation at ambient temperature (no heating), no major differences in the coastdown speed curves are noticeable when supplying the forced cooling flow. On the other hand, at T_{hs}=360ºC, the overall coastdown time reduces by 20% (13 second) with a cooling flow of 50 LPM. At the highest rotor temperature, the forced cooling flow remarkably delays the touchdown speed and increases the overall coastdown time.
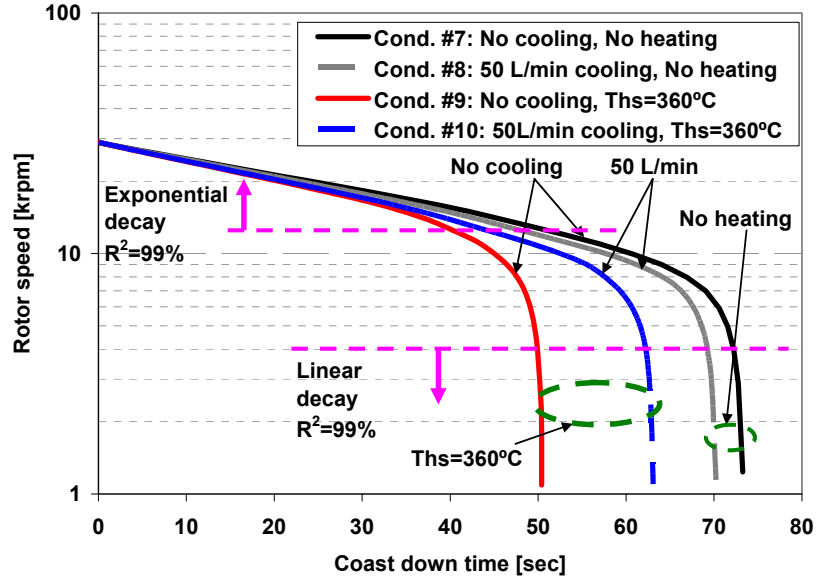
Fig. 16 Test condition 7-10. Effect of cooling flow on time extent for rotor speed coastdown response: Recorded rotor coast down speed versus time with increasing strength of cooling flow and heater temperature. Baseline imbalance.

Post-test condition of test rotor and GFBs

Figure 17 shows (negative) photographs of the test bearings and rotor before and after the tests listed in Table 3 (overall 50 hours of operation). Since the test bearings do not have any protective coatings on their top foil surfaces, wear on the top foil is a critical concern. The majority of the *polished* (wear) marks on the top foil are at its axial edges.

The rotor, originally coated with a 3 micrometer thin dense Chrome layer, shows wear marks at the locations in contact with the bearings, in particular the bearings' outboard edges.

The color of the rotor surface changes along its axes due to the considerable axial temperature gradient, see Appendix A. A higher temperature on the free end rotor OD renders a much darker color on its surface than at the drive end rotor OD.

Transient rubs and contact during start up and shutdown cycles, and predominant rotor conical motions, lead to the large areas of wear on the outboard rotor/bearing edges.
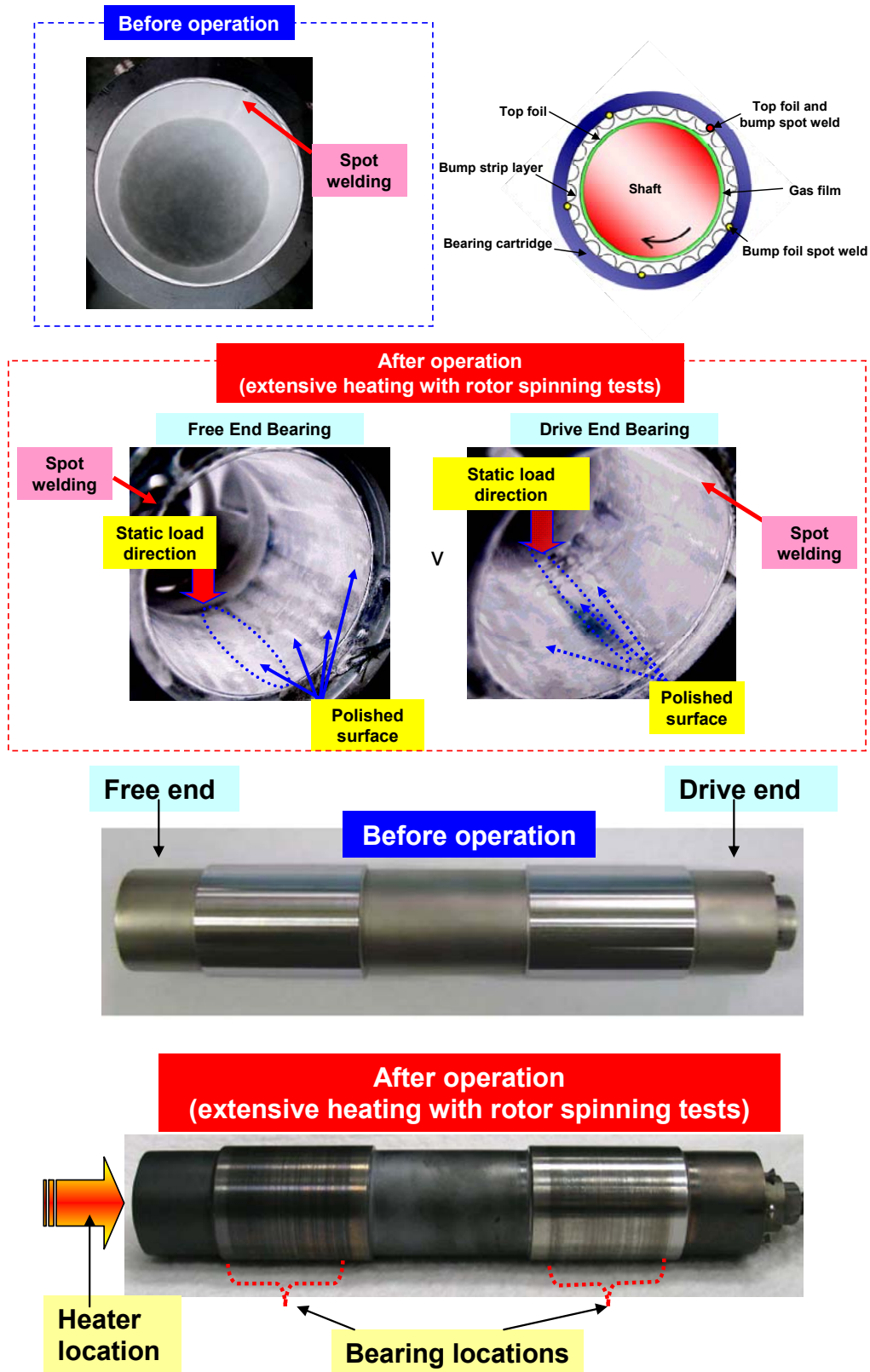
Fig. 17 Surface condition of test GFBs (negative photographs) and rotor after high temperature rotordynamic tests. Overall time of operation=50 hours.

Conclusions

Demonstrated gas foil bearing (GFB) operation at high temperature is fundamental to enable implementation of these bearings into gas turbine applications. Presently, experiments on a hollow test rotor (1.1 kg, 38.1 mm OD, and 25.4 mm ID) supported on two GFBs, 2nd generation, are performed to evaluate the rotordynamic performance of the hot rotor-GFB system while operating at increasing shaft temperatures. An inexpensive electric cartridge, fitting loosely inside the hollow rotor, heats unevenly the rotor.

A series of rotor speed coast downs from 30 krpm demonstrate the rotor response linearity with added imbalance masses. In the current measurements, there are no noticeable differences in rotor response for operation at ambient temperature and at the hottest shaft temperature. While coasting down from 30 krpm to ~11 krpm, the rotor speed decays exponentially, as is typical in systems with viscous drag. As the rotor and bearing temperatures increase, the air becomes more viscous and the bearing clearances decrease; hence the coastdown time somewhat decreases.

The temperatures on the bearing cartridges raise as the rotor temperature increases and also as the operating speed increases. At the hottest test condition, a forced cooling flow stream (at ~23ºC) significantly reduces the bearing temperatures. On the other hand, for operation at ambient or moderately low shaft temperature conditions, a cooling stream is of limited effectiveness. Thermal management with axial cooling streams is beneficial at high temperatures and with large flow rates ensuring turbulent flow conditions.

In gas turbines, an effective thermal management strategy must be ascertained to keep temperatures low, not affecting significantly the material properties of the components, and avoiding excessive thermal gradients, radial and axial. Cold gas bled-off from the compressor is readily available to cool the support bearings and hot rotor. Note that too large cooling rates will reduce engine power output and efficiency, however[11]. Determination of the minimum cooling flow rate for adequate thermal management is an important issue of scrutiny.

The current measurements demonstrate the stability and dynamic forced performance of the rotor-GFB system operating with a hot rotor. The acquired test results will serve to benchmark computational predictive tools near completion [14].

---

[11] Note that the temperature of air at a compressor discharge is relatively high, ~ 150ºC for the low-pressure stage and 343ºC for the high-pressure stage [4].

Proposed work in 2009-2010.

Presently, after completion of the extensive tests detailed above, a 210 V circuit source (rather than 120 V) will power the cartridge heater to convert more electrical power into heat, and hence increase (significantly) the rotor and bearing temperatures. Rotor <u>outer surface</u> temperatures as high as 400ºC are expected.

In 2008, two 2nd generation FBs coated with a patented solid lubricant (Korolon800®, max. 400ºC) were acquired from Mohawk Innovative Technology, Inc. (MiTi®). In addition, one uncoated hollow rotor was manufactured for planned rotordynamic performance tests with the MiTi® GFBs. Therefore, the MiTi® FBs will replace the Foster-Miller FBs. In addition, high temperature fiberoptic displacement sensors[12] (max. 482ºC) will replace the eddy current displacement sensors to enable accurate measurements at high shaft temperatures.

Note that the MiTi® FBs have an outer diameter (44.64 mm) that is smaller than the inner diameter of the bearing holes in the rig housing. Each Miti® GFB fits into an outer shall for insertion into the (original) rig housing, see Fig 18. Each FB outer shell is fitted with four thermocouples on its outer surface.

The rod connecting the drive motor to the test rotor will be shortened to raise the elastic mode critical speed of the rotor-bearing system, thus ensuring safe operation at motor speeds as high as 50 krpm. The experimental results will further aid to anchor the developed predictive tools.

---

[12] Presently, calibrations of the fiberoptic sensors to a new test rotor are completed.
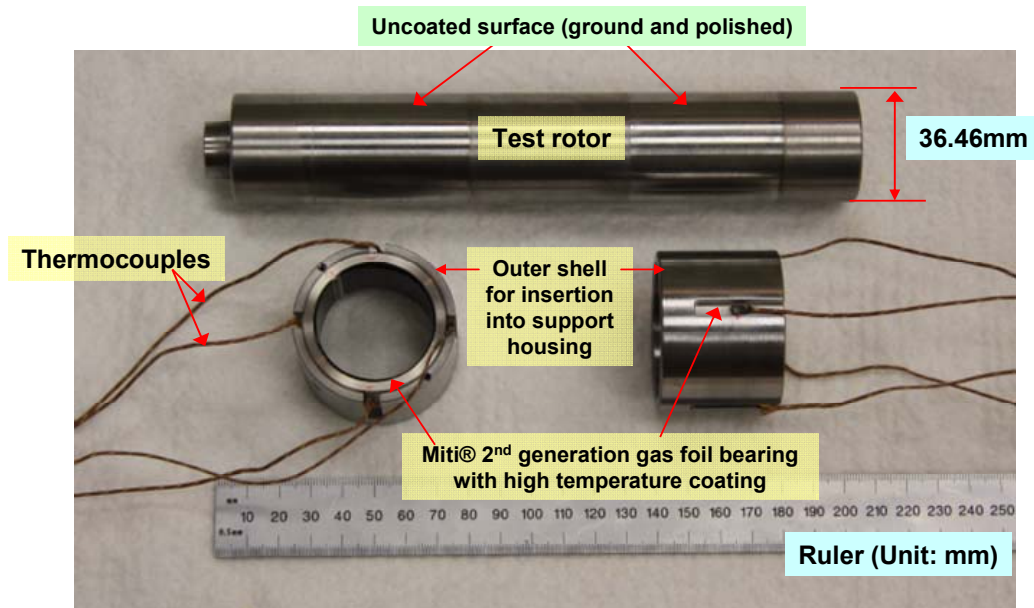
Fig. 18 (new) Test rotor and Miti® GFBs. GFBs in outer shell for installation in test rig housing.

KIST (Korea Institute of Science and Technology) donated one high-speed (high temperature solid lubricant coated, max. 400ºC) Inconel rotor and two pairs of GFB cartridges with 20 bump strips (five different bump heights × four per each height). See Appendix C for details. A series of static load-deflection tests and shaker load tests are being conducted on the KIST foil bearings to determine their structural characteristics. After evaluating the bearing force coefficients, rotordynamic tests will follow.

References

[1] DellaCorte, C., and Valco, M., 2003, "Oil-Free Turbomachinery Technology for Regional Jet, Rotorcraft and Supersonic Business Jet Propulsion Engines," AIAA Paper No. ASABE–2003–1182.

[2] Agrawal, G. L., 1997, "Foil Air/Gas Bearing Technology: An Overview," ASME Paper No. 97-GT-347.

[3] O'Connor, Leo, 1993, "Fluid-film foil bearings control engine heat," Mech. Eng, 115, pp. 72-75.

[4] Radil, K., DellaCorte, C., Zeszotek, M., 2007, "Thermal Management Techniques for Oil-Free Turbomachinery Systems," STLE Tribol. Trans., 50. pp. 319-327.

[5] Dykas, B. D., 2006, "Factors Influencing the Performance of Foil Gas Thrust Bearings for Oil-Free Turbomachinery Applications," Ph.D. Diss., Case Western Reserve University, Cleveland, OH.

[6] Bauman, S., 2005, "An Oil-Free Thrust Foil Bearing Facility Design Calibration, and Operation," NASA/TM-2005-213568.

[7] Heshmat, H., Hryniewicz, P., Walton, J. F., Willis, J. P., Jahanmir, S., DellaCorte, C., 2005, "Low-Friction Wear-Resistant Coatings for High-Temperature Foil Bearings," Tribol. Int., 38, pp. 1059-1075.

[8] Rubio, D., and L., San Andrés, 2006, "Bump-Type Foil Bearing Structural Stiffness: Experiments and Predictions", ASME J. Eng. Gas Turbines Power, 128, pp. 653-660.

[9] Rubio, D., and San Andrés, L., 2007, "Structural Stiffness, Dry Friction Coefficient, and Equivalent Viscous Damping in a Bump-Type Foil Gas Bearing," ASME J. Eng. Gas Turbines Power, 129, pp. 494-502.

[10] San Andrés, L., Rubio, D., and Kim, T.H, 2007, "Rotordynamic Performance of a Rotor Supported on Bump Type Foil Gas Bearings: Experiments and Predictions," ASME J. Eng. Gas Turbines Power, 29(3), pp. 850-857

[11] Breedlove, A., 2007, "Experimental Identification of Structural Force Coefficients in a Bump-Type Foil Bearing," Texas A&M University, M.S. Thesis, College Station, TX.

[12] Kim, T. H., 2007, "Analysis of Side End Pressurized Bump Type Gas Foil Bearings: A Model Anchored to Test Data," Texas A&M University, Ph. D. Diss., College Station, TX.

[13] Kim, T. H., and San Andrés, L., 2008, "Rotordynamic Measurements on a High Temperature Rotor Supported on Gas Foil Bearings," Technical Report No. TRC-B&C-3-08, Texas A&M Univ. College Station, TX.

[14] San Andrés, L., and Kim, T. H., 2008, "Thermohydrodynamic Analysis of Bump Type Gas Foil Bearings: Model and Predictions," Technical Report No. TRC-B&C-2-08, Texas A&M Univ. College Station, TX.

[15] San Andrés, L., Kim, T. H., 2009, "Thermohydrodynamic Model Predictions and Performance Measurements of Bump-type Foil Bearing for Oil-Free Turboshaft Engines in Rotorcraft Propulsion Systems," American Helicopter Society 65th Annual Forum, Grapevine, Texas, May 27- 29, 2009.

[16] San Andrés, L., and Kim, T. H., 2009, Thermohydrodynamic Analysis of Bump Type Gas Foil Bearings: A Model Anchored to Test Data," ASME Paper No. GT2009-59919 (accepted for publication at ASME J. Eng. Gas Turbines Power).

[17] San Andrés, L., and Kim, T. H., 2009, "Forced Nonlinear Response of Gas Foil Bearing Supported Rotors," Tribol. Int., 41, pp. 704-715.

[18] http://www.matweb.com. Accessed May 14, 2009.

[19] Maalouf, M. G., 2007, "Slow Speed Vibration Signal Analysis: If You Can't Do It Slow, You Can't Do It Fast," ASME Paper No. GT2007-28252.

[20] Bently, D.E., 2002, Fundamentals of Rotating Machinery Diagnostics, Bently Pressurized Bearing Company, Minden, NV.

[21] Bachschmid, N., Pennacchi, P., and Vania, A., 2004, "Diagnostic Significance of Orbit Shape Analysis and its Application to Improve Machine Fault Detection," J. Braz. Soc. Mech. Sci. Eng. 26, pp. 200–208.
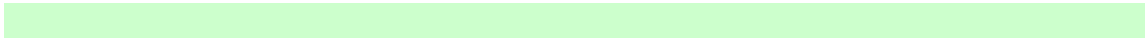
Appendix A. Rotor outer surface temperature at increasing heater temperatures: rotor out of its bearings

The rotor, away from the test rig, hangs from four steel wires. The cartridge heater fits loosely into the hollow portion of the shaft (gap of 4.75mm). The rotor outer surface is exposed to ambient conditions. Temperatures at the rotor OD are recorded for increasingly warmer heater conditions, temperature T_{hs} from 50°C to 400°C with 50°C increments.

Figure A.1 depicts the recorded OD temperatures along the test rotor for increasing heater temperatures (T_{hs}). The figure includes a photograph of the rotor with labels showing the location of the recorded temperatures. To obtain steady state temperature conditions, the heater is powered on during one hour for each heater set temperature (T_{hs}). A high temperature K-type surface probe records the shaft surface temperature. As T_{hs} increases, there is a significant temperature gradient along the rotor axis.
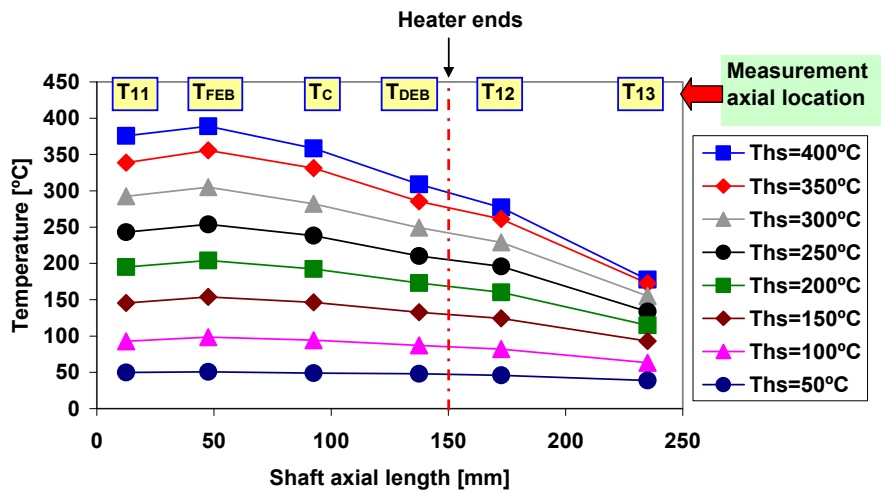
(a) Recorded shaft surface temperatures
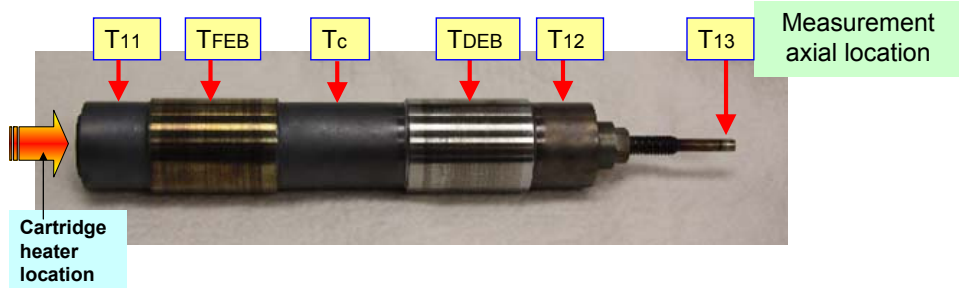
(b) Measurement axial location

Fig. A. 1 (a) Recorded shaft surface temperatures versus axial location for increasing heater set temperature (T_{hs}), and (b) measurement axial locations. Ambient temperature: 21°C.

Appendix B. Specifications and cost of equipment and instrumentation

Table B.1 Specifications and cost of equipment and instrumentation – high temperature rotor GFB test rig

| Item	Specification	Vendor	Model #	Total cost	Delivery
Fiber optic displacement sensor	Tip up to 482°C, cable up to 340°C, sensitivity 2.2mV/μm($1,820×7)	Philtec	RC60-C1T2T9	$12,740	Dec. 07
Infrared thermometer + accessory (mount & laser sighting viewer)	Up to 1370°C, D/S Ratio 68:1, 5Vdc output, adjustable emissivity ($550×2) + $295	OMEGA	OS552-V1-1	$1,295	Dec. 07
Portable infrared thermometer	Up to 538°C, adjustable emissivity	OMEGA	OSXL653,	$100	Dec. 07
Infrared thermo gun		OMEGA	OS423-LS	$148	01/05/08
Thermocouple (K type)	Up to 1090°C, ceramic insulation with Inconel Overbraid ($54×7)	OMEGA	XCIB-K-2-5-10	$378	Jan. 08, Jan. 09
Thermocouple indicator	Up to 1090°C, resolution 0.6°C($195×6)	OMEGA	DP116-KF1	$1,170	Jan. 08
Heater controller	Programmable 1/8 DIN digital panel meter	OMEGA	CNi853	$310	Jan. 08
High temperature foil bearing	1.44" diameter and 1.1" length (with High temperature coating) (2,500×2)	Miti	2nd generation	$5,000	Apr. 08
XY Table with encoder and two axis readout	Travel: 3" X 3" (with encoders) Resolution: 1μm	Velmex	AXY4009 W1	$ 3,753	Mar. 08
High speed motor	9.5kW at 65krpm	KAES	MOO1C80 905	$4,000	Jul. 08
High speed shipping (Intl)	DHL shipping	DHL Express (USA)		$353.34	Aug. 08
Thermocouple (K type)+ Miniature Thermocouple Connectors Flat Pin	Up to 480°C, glass braid insulation ($58×4) ($2.25×6, pin)	OMEGA	5SC-GG-K-30-36, SMPW-K-F	$245.5	Apr. 08, Jan. 09
Insulated thermocouple wire	30m type K duplex insulated wire	OMEGA	PR-K-24-SLE-100	$56	Jan. 09
Cartridge heater	Max. 1.6 kW with 240V	OMEGA	CSH-4101600/240	$76.44	Jul, 08
Cartridge heater	Max. 1 kW with 240V	Thermal Solutions Controls & Indicators	N7A16-10586	$80	Aug. 07
Ceramic fiber paper	Up to 1,200°C	Refractories Incorporated	Kaowool 500	$300	Nov. 07
Hose/connector+AC adapter for flow meter	Air hose and universal AC adapter	Bryan hose and gasket, best buy		$53	May, 08
Steel plate	Cover for instrumentation case 1/8"x4'x8' Smooth Plate cut to length	Mack Bolt and Steel		$150	Jun. 08
Spindle drive	Power source for motor, input 380~480V, 3 phase, 50/60Hz	GMN	90-00124-8048-0000	$4,740	Jul. 08
Heater wire, fuse, switch	Aluminum box, fuse holder and connection, fuse, switch	Mid-State Electronic Supply, McMaster		$159.5	Feb. 08, Jun. 08
Flexible Coupling	Rated torque 1.0 N-m, torsional stiffness 320 N-m/rad($160×3)	R+W coupling technology	MK2/10/33	$480	Sep. 07
Water jet well pump, fittings, hoses	¾ HP, 78 psi, 57L/min	Home Depot	Flotec FP4022	$438.15	Jan. 09
Digital gas mass flow meter, power supply	Max. 500L/min, accuracy ±1.5% of full scale	OMEGA	FMA1844, FMA178PW	$1080	Feb. 09
Socket set screw	Imbalance mass 4-40, ½ length	Ace Bolt & Screw Co.		$4.57	Dec. 08
Step clamp, adjustable height step block	Fixture of heater and bearing support housing	McMaster-Carr	4999A31, 5002A2	$76.17	Dec. 08
Fittings	Connection of gas flow meter	Botco		$4.52	Feb. 09
Power supply	Power of infrared thermometer, 90-264VAC, 24VDC output	OMEGA	PSR-24S	$120	Feb. 09
Reflective tape	For optical tachometer, 1.5m roll, 12 mm wide	OMEGA	HHT-RT-5	$13	Jan. 09

Surface probe	6" length, 1/8" dia.	OMEGA	SPHT-K-6	$45	Jan. 09
Tools	Test rig assembly and maintenance	Harbor freight tools		$257.77	Jan. 09
Switch box, wires	Power system of water pump	Mid-State Electronic Supply, Inc.		$52.47	Jan. 09
Super glue, tape, gloves	Fixture of reflective tape, holding high temperature shaft	Home Depot		$8.78 +$22.53	Jan. 09, Feb. 09
Cost to NASA GRC			Total:	**$37,733.11**	
Shaft + Ni-Cr coating	1.44" diameter (with HT coating)	KIST	High speed rotor	$0 ×1	Dec. 08
High temperature foil bearing	1.44" diameter and 1.1" length	KIST	1st generation	$0 ×4	Dec. 08
Foil bearings repair	1.5" diameter and length (without coating)	Foster Miller Tech.	2nd generation	$3,000 (1,500×2)	Nov. 07
Benchtop thermometer	10-channel benchtop thermometer, dedicated thermocouple input with analog	OMEGA	MDSSi8A-TC	$520×1	Jun. 08
Spindle drive power	Install 480 Volt, 30, 50AMP Power	Texas A&M University	Room134	$465	Aug. 08
Cost other source	(PI incentive)		Total:	**$3,985**	
Hollow shaft	For Miti GFB rotordynamic tests	Vilas Motor Works		$890	Jan. 09
Solid shaft, bearing housing	For KIST GFB static and dynamic load tests.	Vilas Motor Works		$635	Feb. 09
Paid with TRC resources			Total:	**$1,525**	
Total cost				**$43,243.1**	
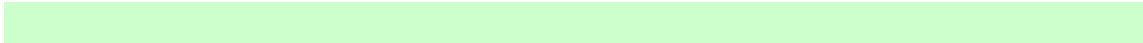
Appendix C. Description of (donated) KIST Foil Bearings

Table C.1 lists the donated KIST rotor and foil bearings. Figure C.1 shows a photograph of (a) all items donated, and (b) the rotor, a connecting rod, a pair of foil bearings, and one (bare) top foil and one bump strip layer. The estimated value of the donated components is $10,000.

There are two sets of bearing cartridges with IDs of 37.95 mm and 37.98 mm. There is a total of 20 bump strip layers, five sets of 4 layers with increasing bump heights, (0.46 mm to 0.54 mm, increments of 0.02 mm). There are six top foils with thickness of 0.12 mm. The number of foil bearing combinations is 10.

Table C.1 List of donated KIST bearings and rotor

| Part		Description	Material	Quantity
Shaft		KIST HT solid lubricant coated. Balancing G0.4.	Inconel 718	1
Connecting rod				4
Nut for connecting rod				4
Bearing cartridge	Set 1	ID: 37.95mm, OD:50.8mm	AISI 4140	2
	Set 2	ID: 37.98mm, OD: 50.8mm		2
Bump strip layer	Set 1	Bump height:0.54mm	Inconel X750	4
	Set 2	Bump height:0.52mm		4
	Set 3	Bump height:0.50mm		4
	Set 4	Bump height:0.48mm		4
	Set 5	Bump height:0.46mm		4
Top foil		Thickness:0.12mm		6
Hex socket screw		Fixture of top foil and bump strip to bearing cartridge		13
Hex key for socket screw				1
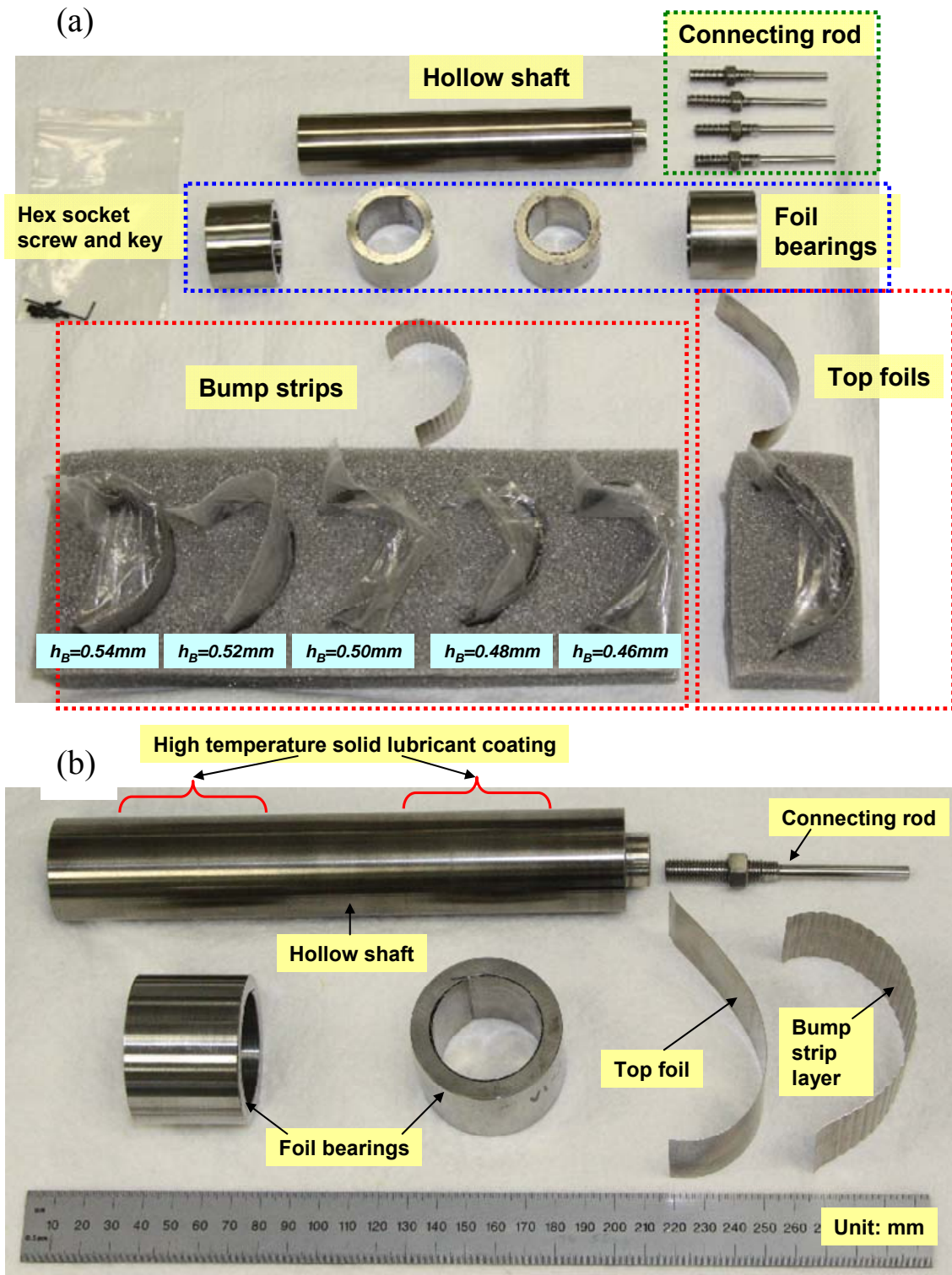
Fig. C.1 Photographs of donated KIST high temperature rotor, foil bearings, top foils and bump strip layers.

Each bearing cartridge accommodates an arcuate top foil and a single bump strip. Underneath the top foil, the bump strip layer has 26 bumps around the bearing circumference.

The leading edges of the top foil and bump strip are free, while their trailing edges are inserted into a narrow slot of the bearing cartridge. Table C.2 lists the measured nominal dimensions of three assembled KIST bearings. The nominal dimensions of the three bearings are identical except for two parameters: bearing V1-1 has a slightly smaller cartridge ID than bearings V2-1 and V2-2, while bearing V2-2 has a slightly smaller bump height than bearings V1-1 and V2-1. Note that the bearing nominal clearance decreases with a smaller ID of the cartridge and a taller bump height.

Table. C.2 Nominal dimensions of three assembled KIST bearings (Unit: mm)

Parameters	V1-1	V2-1	V2-2
Cartridge outer diameter, D_o	50.8	50.8	50.8
Cartridge inner diameter, D_I	**37.95**	37.98	37.98
Axial length, L	38.1	38.1	38.1
Top foil thickness, t_T	0.12	0.12	0.12
Bump foil thickness, t_B	0.12	0.12	0.12
Number of Bumps, N_B	26	26	26
Bump pitch, s_o	4.3*	4.3*	4.3*
Bump length, l_B	2.1*	2.1*	2.1*
Bump height, h_B	0.54	0.54	0.46
Top foil inner diameter, $D_T = D_I - 2(t_T + h_B)$	36.63	36.66	36.82
Young modulus, $E(Gpa)$	209	209	209
Poisson ratio, v	0.284	0.284	0.284
Shaft diameter, D_s	36.555	36.555	36.555
Radial clearance, $C_{nom} = (D_T - D_s)/2$	**0.0375**	**0.0525**	**0.1325**
Weight (lb)	0.60	0.60	0.60

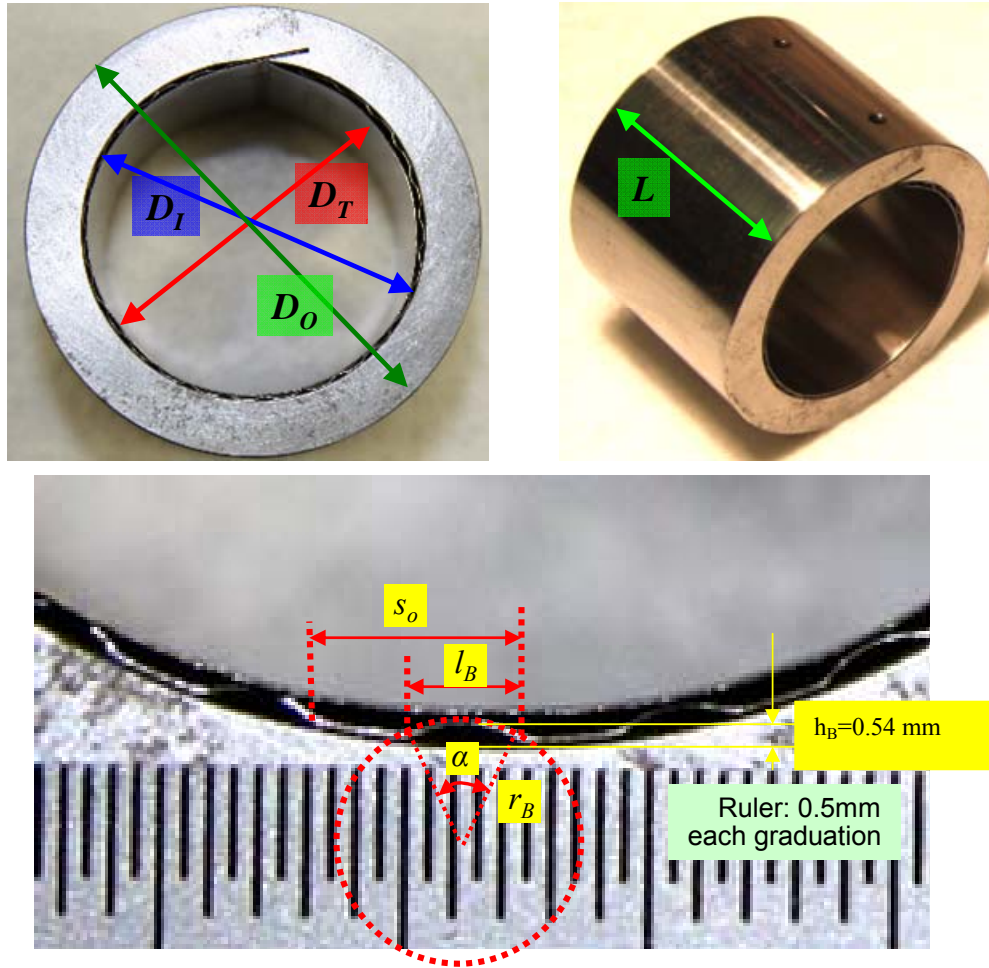* Estimated from zoomed photograph, see Fig. C.2

Fig. C.2 Photographs of one KIST foil bearing (bump height=0.54 mm). Noted dimensions measured or estimated.

Static load versus deflection tests are in progress to determine the foil bearing static structural stiffness coefficient. TRC funds will support further work with these bearings.